

# Baguan-TS: A Sequence-Native In-Context Learning Model for Time Series Forecasting with Covariates

Linxiao Yang<sup>1</sup> Xue Jiang<sup>1</sup> Gezheng Xu<sup>1</sup> Tian Zhou<sup>1</sup> Min Yang<sup>1</sup> Zhaoyang Zhu<sup>1</sup> Linyuan Geng<sup>1</sup>  
Zhipeng Zeng<sup>1</sup> Qiming Chen<sup>1</sup> Xinyue Gu<sup>1</sup> Rong Jin<sup>1</sup> Liang Sun<sup>1</sup>

## Abstract

Transformers enable in-context learning (ICL) for rapid, gradient-free adaptation in time series forecasting, yet most ICL-style approaches rely on tabularized, hand-crafted features, while end-to-end sequence models lack inference-time adaptation. We bridge this gap with a unified framework, Baguan-TS, which integrates the raw-sequence representation learning with ICL, instantiated by a 3D Transformer that attends jointly over temporal, variable, and context axes. To make this high-capacity model practical, we tackle two key hurdles: (i) calibration and training stability, improved with a feature-agnostic, target-space retrieval-based local calibration; and (ii) output oversmoothing, mitigated via context-overfitting strategy. On public benchmark with covariates, Baguan-TS consistently outperforms established baselines, achieving the highest win rate and significant reductions in both point and probabilistic forecasting metrics. Further evaluations across diverse real-world energy datasets demonstrate its robustness, yielding substantial improvements.

## 1. Introduction

Time series forecasting increasingly demands models that adapt swiftly to new tasks, remain robust under distribution shift, and operate efficiently in data-limited regimes. While Transformers have revealed the promise of in-context learning (ICL)—conditioning predictions on a small support set at inference time without gradient updates—most ICL-style approaches in forecasting rely on tabularization and hand-crafted features (Hoo et al., 2025), limiting their ability to exploit the structure of raw sequences. On the other hand, end-to-end sequence models excel at learning representations directly from raw time series but typically lack ICL-style, gradient-free adaptation (Ansari et al., 2024;

<sup>1</sup>DAMO Academy, Alibaba Group, Hangzhou, China.

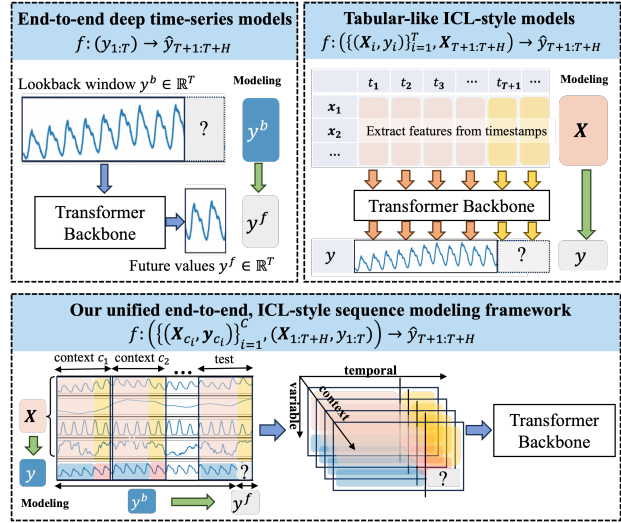


Figure 1. Three paradigms for time series forecasting: (a) End-to-end sequence models learn from raw histories but lack in-context adaptation at inference. (b) Tabular ICL approaches (e.g., TabPFN) perform ICL over feature-engineered representations. (c) Our unified approach (Baguan-TS) enables sequence-native ICL on raw multivariate inputs, attending over temporal, variables, and context for gradient-free adaptation.

Das et al., 2024). This disconnect motivates a framework that unifies end-to-end representation learning with ICL for time series data, so that a single model can both extract features from raw sequences and adapt on the fly.

We propose Baguan-TS, a general-purpose architecture that enables sequence-native ICL on raw multivariate time series without hand-crafted features. It builds on a unified, episodic framework that learns to forecast from raw sequences given a support set, thereby removing dependence on feature engineering while bringing ICL’s rapid adaptation into a sequence-native architecture. An overview of this framework is shown in Fig. 1. To instantiate the framework, we introduce a 3D Transformer that treats **temporal**, **variable**, and **context** dimensions as first-class axes of attention. Analogous to video-style modeling, the model builds multiscale representations over the temporal  $\times$  variable plane and aligns support and query along the context axis via cross-attention. This design lifts the performance ceiling by discovering task-relevant structure directly from raw time se-

ries inputs and specializing predictions per episode through the provided context. In addition, the model admits a 2D inference mode by setting the context length to one, which functions as a strong complementary component in ensembles. In this way, it offers a robust fallback and diversity boost when integrating multiple predictors.

However, adopting a high-capacity 3D architecture introduces two main challenges we target:

**Challenge 1: Locality Calibration.** Large-capacity models are prone to miscalibration and optimization instability, especially when dealing with a large 3D Transformer model. A lightweight, *feature-agnostic* mechanism is needed to provide *local*, episode-specific correction without manual features.

**Challenge 2: Output Oversmoothing in ICL.** In the presence of noisy, heterogeneous support examples, the model can oversmooth the spurious signals rather than extracting stable periodic rules. Effective ICL under these conditions requires a careful balance between *denoising* (resisting noise and shift) and *selection* (focusing on a compact, highly relevant subset of samples).

To improve calibration and stability, we propose a target-space retrieval-based forecast (Y-space RBfcst) local calibration module. By referencing nearest support targets within each episode, this feature-agnostic procedure provides a local, distribution-aware adjustment that complements the learned predictor. It improves calibration and stabilizes training and inference under limited per-task data and distribution shift, and integrates naturally with episodic ICL—offering a simple, retrieval-based bias/variance correction that scales with model capacity without relying on hand-crafted features.

To counter output oversmoothing, we introduce a mitigation strategy that integrates reliability-aware weighting of support examples with deliberately overfitting to some exact context sample in the support set. Counterintuitively, this concentrates attention on the few examples that matter for each query. This balance between denoising and selection reduces spurious correlations and improves few-shot robustness when training a large 3D architecture.

Together, these components form a unified framework that marries representation learning with ICL on raw sequences; a 3D Transformer instantiation that raises the performance (and offers a practical 2D inference mode for ensemble complementarity); and two complementary mechanisms—context-overfitting mitigation and Y-space RBfcst calibration—that make such a high-capacity, ICL-enabled model robust and trainable in practice. The result is a practical route to bringing ICL’s strengths to raw time

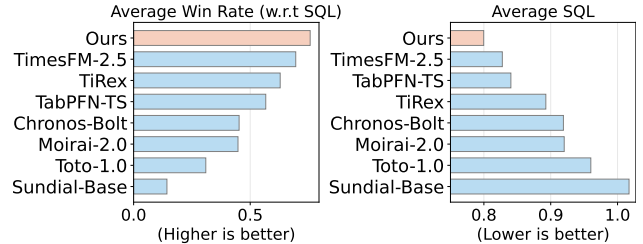


Figure 2. Probabilistic forecasting results on fev-bench-cov (30 covariate-aware tasks): Baguan-TS leads all baselines, achieving the highest average win rate and lowest average SQL.

series forecasting under realistic data and shift conditions. We summarize our contributions as follows:

- We propose Baguan-TS, a unified end-to-end framework that performs ICL directly on raw multivariate time series, without relying on feature engineering. It is instantiated as a 3D Transformer attending jointly over temporal, variable, and context axes, and also supports a 2D inference mode. On fev-bench-cov (30 covariate-aware tasks), Baguan-TS achieves the best average scaled quantile loss (SQL) and MASE with the highest win rate, reducing SQL versus TabPFN-TS by 4.8% (Fig. 2).
- We develop a Y-space RBfcst local calibration module—feature-agnostic and episode-specific—that improves calibration, data efficiency, and scalability when training larger 3D Transformers. In our experiments, this module consistently improves overall forecasting accuracy and robustness under injected noise compared to training without retrieval.
- We introduce a context-overfitting strategy that explicitly balances sample denoising and sample selection, stabilizing in-context learning in high-capacity models. The strategy consistently lowers training loss and restores periodic spike reconstruction, mitigating oversmoothing without harming trend accuracy.

## 2. Related Work

We situate Baguan-TS within three lines of prior work, including end-to-end time series forecasting, large pretrained time series models, and in-context modeling. We summarize the key capability differences of Baguan-TS and these approaches in Table 1.

**Time Series Forecasting.** Deep neural networks dominate modern time series forecasting, with univariate models focusing on single sequences (Rangapuram et al., 2018; Salinas et al., 2020; Oreshkin et al., 2020) and multivariate models jointly modeling many correlated series using

Table 1. Capability comparison of representative time series forecasting approaches.

Models	Raw time sequence	ICL (gradient-free)	No hand-crafted features	Cross-variable interaction	Local retrieval-based calibration
End-to-end models (PatchTST, FedFormer)	✓	×	✓	×	×
Large pretrained models (Chronos, TimesFM, Tirex)	✓	×	✓	×	×
Tabular ICL-style models (TabPFN-TS)	×	✓	×	✓	×
<b>Ours (Baguan-TS)</b>	✓	✓	✓	✓	✓

Transformers (Wu et al., 2021; Zhou et al., 2022b; Nie et al., 2023; Liu et al., 2024a; Wang et al., 2024b; Chen et al., 2024; Zhou et al., 2023) and other architectures (Sen et al., 2019; Zhou et al., 2022a; Jin et al., 2022; Wang et al., 2024a; Hu et al., 2024; Qi et al., 2024). While highly effective on their training domains, these models typically require task-specific retraining, limiting their adaptability and motivating more general-purpose approaches.

**Large Pretrained Time Series Models.** Recent work pre-trains large sequence models for time series (Woo et al., 2024; Goswami et al., 2024; Ansari et al., 2024; Das et al., 2024; Rasul et al., 2023; Liu et al., 2024b; Shi et al., 2025), often with Transformer-based architectures and diverse time series data. However, their zero- and few-shot performance, especially for multivariate forecasting with complex cross-channel dependencies, often still trails specialized models.

**In-Context Modeling.** A complementary line of work treats forecasting as conditional generation and relies on in-context (few-shot) adaptation (Hoo et al., 2025; Feuer et al., 2024; Zhu et al., 2023; Dooley et al., 2023; Hegselmann et al., 2023). While competitive with strong tabular learners, these methods typically rely on hand-crafted features (Chen & Guestrin, 2016; Ke et al., 2017), limiting their practical usages in diverse applications. In contrast, the end-to-end sequence models are preferred by directly capturing temporal structures and cross-channel interactions.

## 3. Baguan-TS

### 3.1. Problem Formulation

In this paper, we consider univariate time series forecasting with known covariates. Let  $\{y_t\}_{t=1}^T$  be the observed series and  $\{\mathbf{x}_t\}_{t=1}^{T+H}$ , where  $\mathbf{x}_t \in \mathbb{R}^M$ , the associated  $M$ -dimensional covariates, available for both the history and the forecast horizon  $H$  (e.g., calendar effects or known exogenous inputs such as weather forecasts). The task is to predict the future values  $\{y_t\}_{t=T+1}^{T+H}$ .

For a test instance, let  $\mathbf{y}^b = (y_{1:T}) \in \mathbb{R}^T$  denote the look-back window,  $\mathbf{y}^f = (y_{T+1:T+H}) \in \mathbb{R}^H$  the future values,

and  $\mathbf{X} \in \mathbb{R}^{(T+H) \times M}$  the covariates over  $t = 1, \dots, T+H$ . We assume an underlying mapping  $\mathbf{y}^f = f^*(\mathbf{y}^b, \mathbf{X})$ .

In the in-context learning setting, we are given a context set  $\mathcal{D}_c = \{(\mathbf{X}_j, \mathbf{y}_j^b, \mathbf{y}_j^f)\}_{j=1}^C$  of  $C$  input-output examples. At test time, we adapt to a target instance by leveraging an inference function  $g$  to approximate  $f^*$ , where the approximation is conditioned on  $\mathcal{D}_c$  to minimize the prediction error  $l(\mathbf{y}^f, g(\mathbf{X}, \mathbf{y}^b, \mathcal{D}_c))$ . Our objective is to learn a universal function  $g$  that can adaptively fit a wide range of different underlying mappings  $f^*$  across diverse tasks.

For convenience, we concatenate covariates and the full series into  $\mathbf{Y}_i = [\mathbf{X}_i, \mathbf{y}_i] \in \mathbb{R}^{(T+H) \times (M+1)}$ , where  $\mathbf{y}_i \in \mathbb{R}^{T+H}$  stacks  $(\mathbf{y}_i^b, \mathbf{y}_i^f)$ . Stacking all context and target samples yields a tensor  $\mathcal{Y} \in \mathbb{R}^{(C+1) \times (T+H) \times (M+1)}$ , whose first  $C$  slices correspond to  $\mathcal{D}_c$  and the last slice to the target instance. For the target slice,  $\mathbf{y}^f$  is unknown and stored as a mask, while it is observed for the context slices.

### 3.2. Architecture

Fig. 3 shows the overall architecture of Baguan-TS, with its components detailed in the following subsections.

#### 3.2.1. PATCHING AND TOKENIZATION

Given the tensor  $\mathcal{Y} \in \mathbb{R}^{(C+1) \times (T+H) \times (M+1)}$ , we apply an encoder based on temporal patching and random Fourier features (Rahimi & Recht, 2007). Each variable in each slice is split along the temporal axis into  $S$  non-overlapping patches of length  $P$  (zero-padding the tail if needed), reducing sequence length while preserving local structure.

For each covariate patch  $\mathbf{q} \in \mathbb{R}^P$ , we map it to  $\mathbf{e} = [\cos(\phi); \sin(\phi)] \in \mathbb{R}^D$ , with  $\phi = \mathbf{W}\mathbf{q} + \mathbf{b}$ , where  $\mathbf{W}$  and

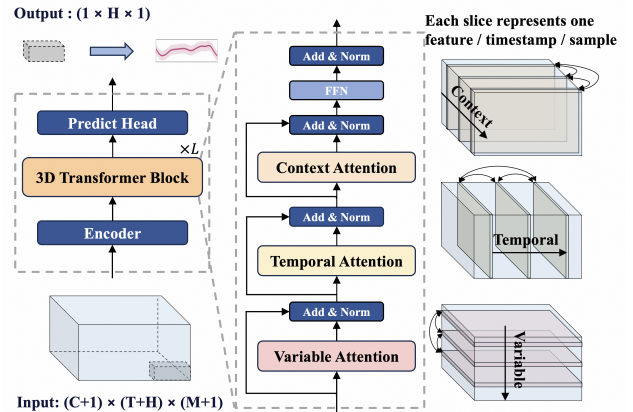


Figure 3. Overall architecture of Baguan-TS. The input tensor  $\mathcal{Y} \in \mathbb{R}^{(C+1) \times (T+H) \times (M+1)}$  is encoded into patch tokens, then iteratively processed by stacked 3D Transformer blocks performing variable, temporal, and context attention, and finally mapped by a prediction head to produce the forecasting outputs  $\mathbf{y}^f \in \mathbb{R}^H$ .

$\mathbf{b}$  are shared learnable parameters. For the target series, we zero-fill the unknown future and use a mask  $\mathbf{m} \in \{0, 1\}^P$  to indicate observed positions. Its embedding  $\mathbf{e}^f$  adds an indicator term  $\mathbf{V}\mathbf{m}$  to the Fourier features to distinguish the history from the forecast horizon. The resulting token tensor has shape  $(C + 1) \times S \times (M + 1) \times D$ .

### 3.2.2. 3D TRANSFORMER BLOCK

The core of our architecture is the 3D Transformer block, an encoder-only module that jointly models correlations across the variable, temporal, and context dimensions. Given the encoded tokens, it applies a sequence of specialized attention layers over these axes, followed by a feed-forward network (FFN). Residual connections and layer normalization follow each attention layer and the FFN.

Compared to conventional 1D or 2D Transformer blocks (Hoo et al., 2025; Ansari et al., 2024) that operate on flattened or reduced-dimensional embeddings, our block preserves a structured three-dimensional layout. This factorized design provides a stronger inductive bias while retaining the flexibility of the standard Transformer.

Formally, let  $\mathbf{Z} \in \mathbb{R}^{(C+1) \times S \times (M+1) \times D}$  denote the token representation (contexts  $\times$  temporal patches  $\times$  variables  $\times$  embedding dimension). All attention layers use standard multi-head self-attention (MHA) (Vaswani et al., 2017) along different axes of this representation. We describe these stages in detail below.

**Temporal Attention.** This module learns temporal dependencies within each context to capture how patterns evolve over time. For each fixed context  $c$  and variable  $m$ , we extract the slice  $\mathbf{T}_{c,m} = \mathbf{Z}_{c,:,m,:} \in \mathbb{R}^{S \times D}$  as the representation along the temporal axis. To model these dependencies, we apply MHA integrated with Rotary Position Embeddings (RoPE). By encoding relative phase information into the query and key vectors, RoPE allows the mechanism to naturally capture relative temporal distances and periodic patterns, which are crucial for time series forecasting.

**Variable Attention:** Instead of temporal sequences, this branch operates on the variable dimension  $\mathbf{V}_{c,s} = \mathbf{Z}_{c,s,:} \in \mathbb{R}^{(M+1) \times D}$  for each time step  $s$ . To account for distinct variable semantics, we augment the representation with a learnable variable-wise embeddings before performing MHA to capture cross-variable correlations.

**Context Attention:** This branch models relationships across different instances by taking the slice  $\mathbf{C}_{s,m} = \mathbf{Z}_{:,s,m,:} \in \mathbb{R}^{(C+1) \times D}$ . Unlike the temporal and variable branches, context attention omits positional encodings, as the context dimension typically lacks an inherent sequential ordering and instead focuses on global information sharing.

### 3.2.3. PREDICTION HEAD

After a stack of 3D Transformer blocks, we obtain latent representations for future patches. A lightweight MLP head maps these features to per-horizon predictive distributions. Because inputs are  $z$ -normalized on the lookback (approximately zero mean and unit variance), most forecast values lie within a bounded range; we fix  $[-10, 10]$  and uniformly discretize it into  $K = 5000$  bins. For each horizon step, the head outputs logits over these bins; applying softmax yields a probability vector  $\mathbf{p} \in \mathbb{R}^K$ . This provides a full probabilistic forecast with both point estimates (via the expected value over bin centers) and quantiles (via the empirical CDF).

## 3.3. Training

Our 3D Transformer operates on context–target episode sets. During training, we (i) build these contexts via retrieval-based forecasting; and (ii) stabilize in-context learning with a context-overfitting strategy. Implementation details on training data, loss functions, and inference settings are in Appendix A.

### 3.3.1. RETRIEVAL-BASED FORECASTING

To construct informative and scalable contexts, we adopt retrieval-based forecasting (Rbfcst) to select informative contexts at scale. For a series of length  $N$  and a context window  $T + H$ , there are  $N - T - H + 1$  candidate subsequences of length  $T + H$ , so full enumeration is memory-intensive. Instead, given the target lookback  $\mathbf{y}^b \in \mathbb{R}^T$  as the query, we retrieve its  $K_{\text{ctx}}$  nearest  $T$ -length subsequences from a sliding-window index over the historical region (to avoid leakage). Each retrieved  $T$ -length window, together with the subsequent  $H$  points, forms one context of length  $T + H$  (with covariates aligned). Distances are computed on  $z$ -normalized windows (e.g., Euclidean or cosine), and  $K_{\text{ctx}}$  is chosen to balance relevance and memory.

To align training with this strategy and increase diversity, we first select a reference sequence of length  $T + H$ , sample a lookback of length  $T$ , and retrieve  $2K_{\text{ctx}}$  nearest  $T$ -length subsequences using the same procedure. This leads to  $2K_{\text{ctx}} + 1$  candidates (including the selected reference), which is stacked into a tensor of shape  $(2K_{\text{ctx}} + 1) \times S \times (M + 1)$ . We then randomly choose  $K_{\text{ctx}}$  slices to form a tensor of shape  $K_{\text{ctx}} \times S \times (M + 1)$  for that step. A subset of these  $K_{\text{ctx}}$  slices is designated as the target (with its future masked), and the remainder serve as context. This randomized subsampling from a larger pool mimics imperfect retrieval, encouraging context diversity and robustness to retrieval noise.

Related tabular foundation models (Thomas et al., 2024; Xu et al., 2025; Gorishniy et al., 2024) typically retrieve in covariate space ( $\mathbf{X}$ -space). In contrast, we retrieve by

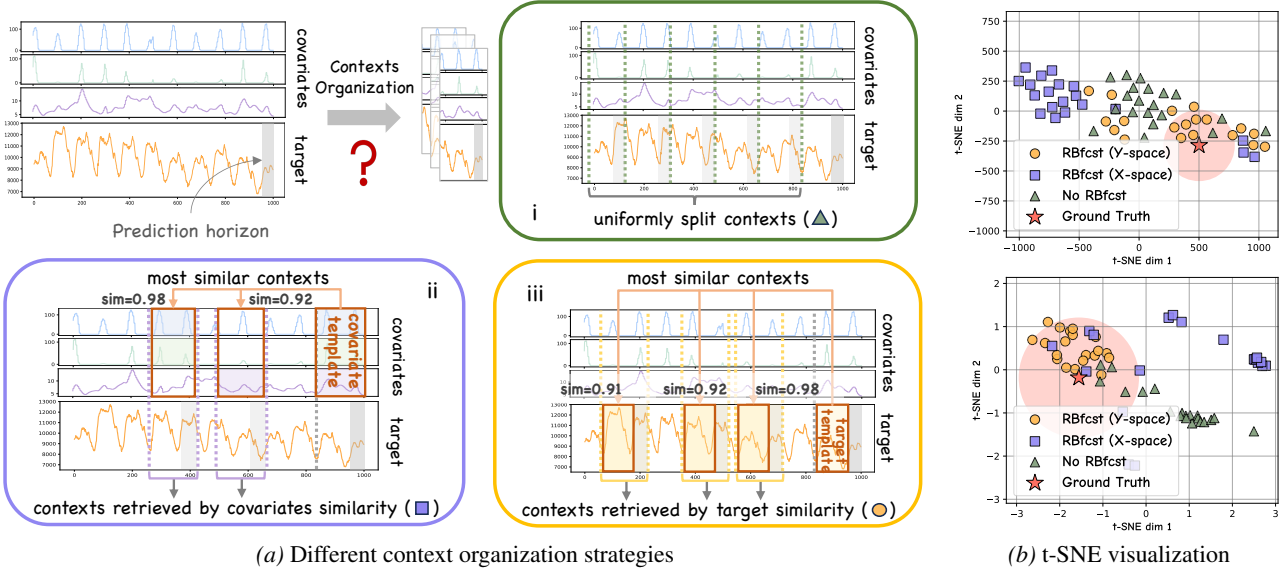


Figure 4. Context organization strategies and t-SNE visualization. (a) Three context organization methods: (i) uniform splits (green); (ii) covariate-based retrieval in X-space (purple, relies on feature engineering); (iii) target-based retrieval in Y-space (ours, yellow), which focuses on historical patterns and is feature-agnostic. Higher similarity scores indicate stronger contextual relevance. (b) t-SNE plots of prediction horizons on *epf* (top) and *ent\_soe* (bottom) for three RBfcst variants. The ground truth (red star) lies closest to the Y-space RBfcst cluster (shaded), indicating it best captures the true pattern.

similarity of the target history (Y-space), i.e., nearest neighbors of the lookback segment. For time series, the trajectory often summarizes the combined effects of all drivers, making Y-space retrieval more informative and feature-agnostic, without hand-crafted feature design.

To illustrate robustness, we compare three context-organization strategies in Fig. 4: (i) uniform splitting (green), where windows are taken at equal intervals; (ii) X-space retrieval (purple), guided by covariate similarity and feature engineering; and (iii) Y-space retrieval (yellow, ours), which focuses on historical patterns most similar to the target. Higher similarity scores indicate stronger contextual relevance. t-SNE plots on *epf* (top) and *ent\_soe* (bottom) show that horizons retrieved in Y-space cluster near the ground truth (red star), suggesting this strategy best captures the true pattern.

### 3.3.2. CONTEXT-OVERFITTING STRATEGY

The direct application of in-context learning to time series forecasting reveals a critical limitation: during early training, models tend to predict smooth, low-frequency trends while systematically suppressing periodic spike signals. This happens even when identical spike patterns are clearly present in the context window, indicating that the model misinterprets such abrupt fluctuations as noise rather than valid signal components. Although this tendency may enhance robustness against irregular outliers in certain datasets, it severely undermines performance in time series domains where pe-

riodic spikes constitute essential features (e.g., physiological monitoring or demand surges). To mitigate this over-smoothing issue where the model fails to leverage contextual spike templates for query inference, we introduce a context-overfitting strategy. Concretely, we enrich the query with a short segment copied verbatim from one context slice and add an auxiliary self-retrieval objective: the model is required to identify and align the matching context segment and reconstruct the corresponding target values (see Fig. 5, where we include a synthetic test sample  $x_2$  whose lookback contains a motif duplicated from the context, and train the model to retrieve that context). This explicitly encourages template matching: model must identify and retrieve target

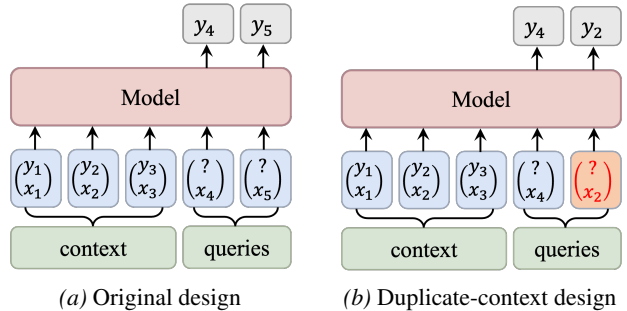


Figure 5. Illustration of the context-overfitting strategy. (a) Original design, where the model forecasts query targets from retrieved context episodes. (b) Duplicate-context design: a short segment from one context slice is copied into a query, and the model is trained to retrieve the matching context and reconstruct its targets.

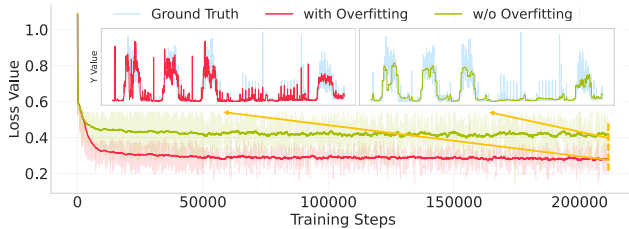


Figure 6. Effect of the context-overfitting strategy. Main: training loss curves for the baseline model (green) and our context-overfitting strategy (red). Insets: example forecasts compared with ground truth (blue). The baseline oversmooths outputs and misses high-frequency spikes (right); our strategy keeps a low loss while recovering spike patterns by matching contextual templates (left).

values from the context when encountering identical patterns in the query. As demonstrated by the training dynamics and qualitative results in Fig. 6, the baseline model underutilizes contextual templates and produces oversmoothed predictions, while our strategy enables accurate reconstruction of periodic spikes without compromising trend accuracy.

### 3.4. Adaptive Inference

A key property of the 3D Transformer is its structural flexibility: it can operate either as a full sequence-native model or as a 2D tabular-style predictor. Setting the context length  $S = 1$  collapses the temporal axis and restrict attention to feature and context dimensions. We find this 2D mode useful when temporal dependence is mostly captured by covariates or is weak (e.g., unreliable history under distribution shift). Thus, we ensemble the 2D and 3D modes in inference, which consistently improves SQL and reduces quantile calibration errors compared to using either mode alone.

## 4. Experiments

### 4.1. Experiment Settings

We compare Baguan-TS with recent time series foundation models: Sundial-Base (Liu et al., 2025b), TabPFN-TS (Hoo et al., 2025), TimesFM-2.0 (Das et al., 2024), TiRex (Auer et al., 2025), Toto-1.0 (Cohen et al., 2025), Chronos-Bolt (Ansari et al., 2024), and Moirai-2.0 (Liu et al., 2025a). Among them, only TabPFN-TS natively supports covariates; models without covariate support are evaluated on target-only inputs.

We report mean absolute scaled error (MASE), weighted absolute percentage error (WAPE), scaled quantile loss (SQL), and weighted quantile loss (WQL), and the corresponding average win rates for each metric (Shchur et al., 2025), averaged over horizons and macro-averaged across datasets. Further details of the datasets, experimental setup, and additional results are provided in Appendices B and C.

### 4.2. Zero-Shot Forecasting

#### 4.2.1. TIME SERIES FORECASTING WITH COVARIATES

**Evaluation on public datasets.** We first evaluate Baguan-TS on the `fev-bench` benchmark (Shchur et al., 2025). Focusing on time series tasks with covariate information, we select 30 representative tasks from the 100 available datasets that provide at least one known dynamic covariate, and refer to this subset as `fev-bench-cov`. We evaluate both point and probabilistic forecasting performance, comparing Baguan-TS against leading time series foundation models. The results are reported in Fig. 2 and Figs. 18–20 (Appendix C.1). As shown in Table 2, Baguan-TS consistently outperforms both univariate baselines, including TiRex and Toto-1.0, and models specifically designed for covariate-informed forecasting, such as TabPFN-TS. This demonstrates Baguan-TS can effectively leverage both historical target series and future covariates for accurate predictions.

Table 2. Average results on `fev-bench-cov`. The best results are highlighted in **bold**, and the second-best results are underlined.

Model	SQL	MASE	WAPE	WQL
Chronos-Bolt	0.9190	1.1233	0.2702	0.2181
Moirai-2.0	0.9202	1.1233	0.2750	0.2226
Sundial-Base	1.0172	1.1449	0.2813	0.2498
TimesFM-2.5	<u>0.8276</u>	<u>1.0122</u>	0.2592	0.2095
TabPFN-TS	0.8404	1.0430	<b>0.2015</b>	<b>0.1643</b>
TiRex	0.8927	1.1081	0.2753	0.2233
Toto-1.0	0.9600	1.1755	0.2737	0.2248
Ours	<b>0.7997</b>	<b>0.9857</b>	<u>0.2173</u>	<u>0.1724</u>

**Evaluation on real-world applications.** We further evaluate Baguan-TS on 27 real-world datasets with historical and future covariates (e.g., weather, calendar). Table 3 reports averages over all datasets. Among the baselines, only TabPFN-TS and Baguan-TS use covariates; the others operate on the target series only. Baguan-TS achieves the best overall SQL, MASE, WAPE, and WQL, improving over TabPFN-TS and all non-covariate baselines, indicating more effective use of contextual signals. Detailed dataset descriptions and experimental results are provided in the Appendix C.1.

#### 4.2.2. UNIVARIATE TIME SERIES FORECASTING

We next consider univariate time series forecasting without covariates, where Baguan-TS adapts by incorporating null or time-only feature columns. Specifically, we evaluated 10 tasks from the `fev-bench-mini` dataset (Shchur et al., 2025), where multivariate datasets are flattened into standard univariate forecasting problems; we refer to this subset as `fev-bench-uni`. As shown in Fig. 7, Baguan-TS achieves competitive macro-averaged SQL across tasks even without covariates. Notably, it outperforms TabPFN-

Table 3. Average results on real-world application datasets. The best results are highlighted in **bold**, and the second-best results are underlined.

Model	SQL	MASE	WAPE	WQL
Chronos-Bolt	0.5101	0.6350	0.0976	0.0783
Moirai-2.0	0.7139	0.8875	0.1031	0.0860
Sundial-Base	0.7486	0.9042	0.1133	0.0981
TabPFN-TS	<u>0.4663</u>	<u>0.6115</u>	<u>0.0688</u>	<u>0.0537</u>
TimesFM-2.0	0.8418	0.9278	0.1093	0.0954
TiRex	0.5710	0.7094	0.0975	0.0784
Toto-1.0	0.8414	1.0566	0.1269	0.1034
Ours	<b>0.3974</b>	<b>0.4956</b>	<b>0.0597</b>	<b>0.0490</b>

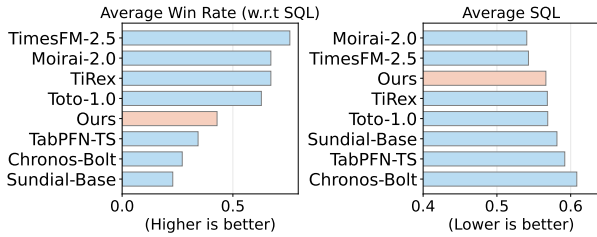


Figure 7. Evaluation on *fev-bench-uni* (10 univariate/multivariate tasks). Baguan-TS achieves competitive probabilistic forecasting performance on tasks without covariates.

TS, which also natively supports covariates, on more than 50% of these datasets; it also achieves SOTA performance in terms of macro-averaged WAPE and WQL (see Fig. 21, Appendix C.2). These results indicate strong macro-level stability and robustness on aggregate-sensitive metrics, highlighting system-level accuracy.

### 4.3. Ablation Study

#### 4.3.1. EFFECT OF RBFCST

We first ablate the proposed RBfcst module on an energy task (*entsoe\_1h*) and a retail task (*hermes*). The baseline (w/o RBfcst) uses uniformly split contexts. We compare three retrieval variants: X-space (covariates), XY-space (covariates + targets), and our Y-space RBfcst (targets only). All variants use the average of cosine and  $L_2$  distances for segment similarity.

As shown in Table 4, Y-space RBfcst consistently outperforms both X-space and XY-space variants, all of which significantly surpass the w/o RBfcst baseline. This validates the critical role of RBfcst in ICL-based time series forecasting and confirms that historical target trajectories generally provide more informative context than covariates, without requiring sophisticated feature selection or aggregation mechanisms. The performance advantage of Y-space RBfcst is particularly large on *entsoe\_1h*, whereas the gap is smaller on *hermes*, which has shorter lookback windows and sparser covariates.

Table 4. Probabilistic and point forecasting evaluation for different RBfcst variants on *entsoe\_1h* and *hermes* datasets.

Method	<i>entsoe_1h</i>				<i>hermes</i>			
	SQL	MASE	WAPE	WQL	SQL	MASE	WAPE	WQL
w/o RBfcst	0.4284	0.5387	0.0328	0.0262	0.6607	0.8445	0.0032	0.0025
X-space	0.4185	0.5178	0.0313	0.0256	0.6186	0.7973	0.0030	0.0023
XY-space	0.4005	0.4972	0.0297	0.0241	0.6186	0.7972	0.0030	0.0023
Y-space	0.3859	0.4819	0.0287	0.0231	0.6185	0.7971	0.0030	0.0023

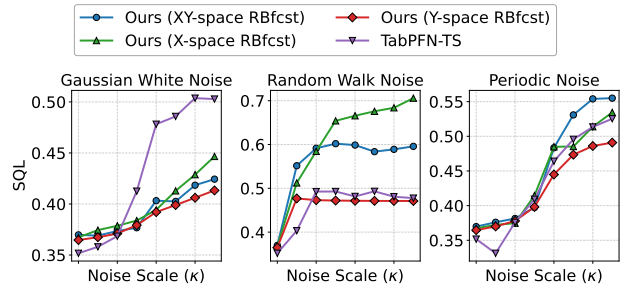


Figure 8. Robustness evaluation on *epf\_fr* under Gaussian white noise, random walk noise, and periodic noise, with  $\kappa \in \{0, 0.05, 0.1, 0.2, 0.4, 0.6, 0.8, 1.0\}$ .

To further evaluate the robustness of our local calibration module, we conduct noise-injection experiments on *epf\_fr* using three representative noise types: (i) Gaussian white noise (stationary); (ii) random walk noise (non-stationary with trend); and (iii) periodic noise (seasonal interference). The noise intensity is controlled by a scaling factor  $\kappa$  relative to the series’ empirical standard deviation (see Appendix B.2 for details). As shown in Fig. 8, although TabPFN-TS achieves the best SQL in the clean setting ( $\kappa = 0$ ), its performance degrades sharply under stationary Gaussian noise as  $\kappa$  increases (especially when  $\kappa \geq 0.1$ ). In contrast, Baguan-TS maintains stable performance across all noise types and intensities. Notably, the Y-space RBfcst variant exhibits the highest robustness, with minimal performance drop even at high noise levels. This shows that our feature-agnostic locality calibration effectively mitigates the impact of diverse external perturbations.

#### 4.3.2. EFFECT OF CONTEXT-OVERFITTING

We ablate the proposed context-overfitting strategy by re-training two models (a full model with context-overfitting and a baseline without it) from scratch for 220K steps on a dataset with clear daily and weekly seasonality and periodic spikes. Fig. 6 shows training losses and qualitative forecasts. With context-overfitting, the training loss is consistently lower—unsurprising, as the auxiliary self-retrieval task (recovering targets for a query containing a duplicated context segment) is easier than forecasting unseen targets. More importantly, without context-overfitting the forecasts are overly smooth and miss most spikes, while the full model

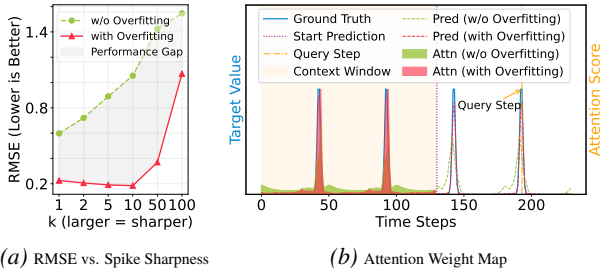


Figure 9. Ablation of the context-overfitting strategy. (a) The full model (red) consistently outperforms the baseline (green) on synthetic periodic spike data for all  $k$ , where larger  $k$  corresponds to sharper spikes. (b) Attention map for a representative peak step (orange dotted line).

captures much more high-frequency structure and accurately predicts the periodic spikes without distorting the trend.

To further assess robustness and clarify the mechanism, we compare these two models on synthetic periodic toy data. As shown in Fig. 9a, the full model substantially reduces RMSE and more consistently recovers periodic spikes from the lookback window. To examine attention behavior, Fig. 9b visualizes a local attention map: with context-overfitting, the peak step attends strongly to historical peaks, whereas the baseline exhibits a pronounced dip at these locations, supporting our explanation of over-smoothing in vanilla attention. Details of the data generation and additional visualizations are provided in Appendix B.3.

### 4.3.3. DIFFERENT INFERENCE MODES

In this section, we compare the 2D, 3D, and ensemble inference modes. Averaged results on the `fev-bench-cov` are presented in Table 5. While the standalone 3D and 2D modes already deliver strong performance, their ensemble consistently improves all metrics for both point and probabilistic forecasting. To understand these gains, we compute the Pearson correlation between 2D and 3D residuals pooled across all tasks (Fig. 10a), obtaining 0.75. This confirms that both modes are accurate and successfully capture the dominant temporal dynamics, while the correlation being well below 1.0 indicates diverse error structures. To further visualize this diversity, we plot the joint residual distribution for the `entsoe_1H` task in Fig. 10b, where points in the second and fourth quadrants highlight opposite-signed residuals, suggesting complementary errors. We also evaluate

Table 5. Average results on `fev-bench-cov` under different inference modes of Baguan-TS model.

Model	SQL	MASE	WAPE	WQL
Ours (2D mode)	0.8769	1.0705	0.2333	0.1863
Ours (3D mode)	0.8333	1.0220	0.2285	0.1830
Ours (Ensemble)	0.7997	0.9857	0.2173	0.1724

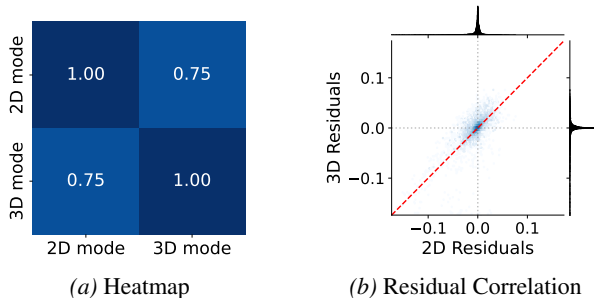


Figure 10. Residual correlation analysis of 2D and 3D inference modes. (a) Aggregated Pearson correlation across 30 tasks in `fev-bench-cov`. (b) Joint residual distribution for `entsoe_1H`, where darker blue bins indicate higher data density. Points along the red dashed identity line ( $y = x$ ) represent cases in which the errors in both modes are equal. Deviations from this diagonal, particularly in the second and fourth quadrants, highlight the complementary error structures between the two modes.

the probabilistic calibration using calibration histograms (Fig. 11) (Gneiting et al., 2007). The x-axis shows ground-truth quantile levels under predicted CDFs; perfectly calibrated models yield a uniform histogram. We observe opposite systematic biases in the base modes: the 2D mode shows a peaked histogram indicating under-confident predictions, whereas the 3D mode exhibits a U-shape distribution with over-confidence. The ensemble mode balances these errors, yielding a near-uniform histogram for better calibration.

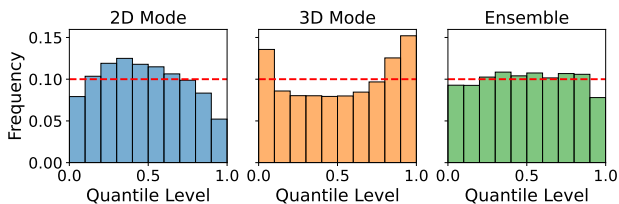


Figure 11. Calibration histograms of ground-truth quantile levels in predicted CDFs for different inference modes on `entsoe_1H`. A well-calibrated model yields a uniform histogram (red dashed line). The 2D mode is under-confident (peaked), the 3D mode is over-confident (U-shaped), whereas the ensemble effectively cancels these biases and approaches the ideal uniform distribution.

## 5. Conclusion

We presented Baguan-TS, a unified framework that brings in-context learning to raw time series by combining a 3D Transformer over temporal, variable, and context axes with a practical 2D+3D inference scheme. A target-space retrieval-based calibration module and a context-overfitting strategy make this high-capacity architecture more stable, better calibrated, and less prone to oversmoothing. Across `fev-bench-cov`, `fev-bench-uni` and 27 in-house datasets, Baguan-TS consistently exhibits strong performance, showing that raw-sequence ICL can be both effective and robust in realistic forecasting settings.

## References

- Aksu, T., Woo, G., Liu, J., Liu, X., Liu, C., Savarese, S., Xiong, C., and Sahoo, D. Gift-eval: A benchmark for general time series forecasting model evaluation. *arXiv preprint arXiv:2410.10393*, 2024.
- Ansari, A. F., Stella, L., Turkmen, C., Zhang, X., Mercado, P., Shen, H., Shchur, O., Rangapuram, S. S., Arango, S. P., Kapoor, S., et al. Chronos: Learning the language of time series. *arXiv preprint arXiv:2403.07815*, 2024.
- Auer, A., Podest, P., Klotz, D., Böck, S., Klambauer, G., and Hochreiter, S. Tirez: Zero-shot forecasting across long and short horizons with enhanced in-context learning. *arXiv preprint arXiv:2505.23719*, 2025.
- Chang, K.-M. Arrhythmia ECG noise reduction by ensemble empirical mode decomposition. *Sensors*, 10(6): 6063–6080, 2010.
- Chen, P., Zhang, Y., Cheng, Y., Shu, Y., Wang, Y., Wen, Q., Yang, B., and Guo, C. Pathformer: Multi-scale transformers with adaptive pathways for time series forecasting. In *Proceedings of the International Conference on Learning Representations*, 2024.
- Chen, T. and Guestrin, C. XGBoost: A scalable tree boosting system. In *Proceedings of the 22nd ACM SIGKDD International Conference on Knowledge Discovery and Data Mining*, pp. 785–794, 2016.
- Cohen, B., Khwaja, E., Doubli, Y., Lemaachi, S., Lettieri, C., Masson, C., Miccinilli, H., Ramé, E., Ren, Q., Ros-tamizadeh, A., et al. This time is different: An observability perspective on time series foundation models. *arXiv preprint arXiv:2505.14766*, 2025.
- Das, A., Kong, W., Sen, R., and Zhou, Y. A decoder-only foundation model for time-series forecasting. In *Proceedings of the 41st International Conference on Machine Learning*, 2024.
- Dooley, S., Khurana, G. S., Mohapatra, C., Naidu, S. V., and White, C. ForecastPFN: Synthetically-trained zero-shot forecasting. *Advances in Neural Information Processing Systems*, 36:2403–2426, 2023.
- Feuer, B., Schirrmester, R. T., Cherepanova, V., Hegde, C., Hutter, F., Goldblum, M., Cohen, N., and White, C. TuneTables: Context optimization for scalable prior-data fitted networks. *Advances in Neural Information Processing Systems*, 37:83430–83464, 2024.
- Gneiting, T., Balabdaoui, F., and Raftery, A. E. Probabilistic forecasts, calibration and sharpness. *Journal of the Royal Statistical Society Series B: Statistical Methodology*, 69 (2):243–268, 2007.
- Gorishniy, Y., Rubachev, I., Kartashev, N., Shlenskii, D., Kotelnikov, A., and Babenko, A. TabR: Tabular deep learning meets nearest neighbors. In *Proceedings of the 12th International Conference on Learning Representations*, 2024.
- Goswami, M., Szafer, K., Choudhry, A., Cai, Y., Li, S., and Dubrawski, A. MOMENT: A family of open time-series foundation models. In *Proceedings of the 41st International Conference on Machine Learning*, 2024.
- Hegselmann, S., Buendia, A., Lang, H., Agrawal, M., Jiang, X., and Sontag, D. TabLLM: Few-shot classification of tabular data with large language models. In *Proceedings of the 26th International Conference on Artificial Intelligence and Statistics*, pp. 5549–5581, 2023.
- Hoo, S. B., Müller, S., Salinas, D., and Hutter, F. The tabular foundation model TabPFN outperforms specialized time series forecasting models based on simple features. *arXiv preprint arXiv:2501.02945*, 2025.
- Hu, J., Hu, Y., Chen, W., Jin, M., Pan, S., Wen, Q., and Liang, Y. Attractor memory for long-term time series forecasting: A chaos perspective. *Advances in Neural Information Processing Systems*, 37:20786–20818, 2024.
- Jin, M., Zheng, Y., Li, Y.-F., Chen, S., Yang, B., and Pan, S. Multivariate time series forecasting with dynamic graph neural odes. *IEEE Transactions on Knowledge and Data Engineering*, 35(9):9168–9180, 2022.
- Ke, G., Meng, Q., Finley, T., Wang, T., Chen, W., Ma, W., Ye, Q., and Liu, T.-Y. LightGBM: A highly efficient gradient boosting decision tree. *Advances in Neural Information Processing Systems*, 30, 2017.
- Kim, G. I. and Chung, K. Extraction of features for time series classification using noise injection. *Sensors*, 24 (19):6402, 2024.
- Kim, T., Kim, J., Tae, Y., Park, C., Choi, J.-H., and Choo, J. Reversible instance normalization for accurate time-series forecasting against distribution shift. In *Proceedings of the International Conference on Learning Representations*, 2022.
- Liu, C., Aksu, T., Liu, J., Liu, X., Yan, H., Pham, Q., Sahoo, D., Xiong, C., Savarese, S., and Li, J. Moirai 2.0: When less is more for time series forecasting. *arXiv preprint arXiv:2511.11698*, 2025a.
- Liu, Y., Hu, T., Zhang, H., Wu, H., Wang, S., Ma, L., and Long, M. iTransformer: Inverted transformers are effective for time series forecasting. In *Proceedings of the 12th International Conference on Learning Representations*, 2024a.

- Liu, Y., Zhang, H., Li, C., Huang, X., Wang, J., and Long, M. Timer: Generative pre-trained transformers are large time series models. In *Proceedings of the 41st International Conference on Machine Learning*, 2024b.
- Liu, Y., Qin, G., Shi, Z., Chen, Z., Yang, C., Huang, X., Wang, J., and Long, M. Sundial: A family of highly capable time series foundation models. *arXiv preprint arXiv:2502.00816*, 2025b.
- Nie, Y., Nguyen, N. H., Sinthong, P., and Kalagnanam, J. A time series is worth 64 words: Long-term forecasting with transformers. In *Proceedings of the 11th International Conference on Learning Representations*, 2023.
- Oreshkin, B. N., Carпов, D., Chapados, N., and Bengio, Y. N-beats: Neural basis expansion analysis for interpretable time series forecasting. In *Proceedings of the International Conference on Learning Representations*, 2020.
- Qi, S., Xu, Z., Li, Y., Wen, L., Wen, Q., Wang, Q., and Qi, Y. PDETime: Rethinking long-term multivariate time series forecasting from the perspective of partial differential equations. *arXiv preprint arXiv:2402.16913*, 2024.
- Rahimi, A. and Recht, B. Random features for large-scale kernel machines. *Advances in Neural Information Processing Systems*, 20, 2007.
- Rangapuram, S. S., Seeger, M. W., Gasthaus, J., Stella, L., Wang, Y., and Januschowski, T. Deep state space models for time series forecasting. *Advances in Neural Information Processing Systems*, 31, 2018.
- Rasul, K., Ashok, A., Williams, A. R., Khorasani, A., Adamopoulos, G., Bhagwatkar, R., Biloš, M., Ghonia, H., Hassen, N. V., Schneider, A., Garg, S., Drouin, A., Chapados, N., Nevmyvaka, Y., and Rish, I. Lag-Llama: Towards foundation models for time series forecasting. *arXiv preprint arXiv:2310.08278*, 2023.
- Salinas, D., Flunkert, V., Gasthaus, J., and Januschowski, T. DeepAR: Probabilistic forecasting with autoregressive recurrent networks. *International Journal of Forecasting*, 36(3):1181–1191, 2020.
- Sen, R., Yu, H.-F., and Dhillon, I. S. Think globally, act locally: A deep neural network approach to high-dimensional time series forecasting. *Advances in Neural Information Processing Systems*, 32:4837–4846, 2019.
- Shchur, O., Ansari, A. F., Turkmen, C., Stella, L., Erickson, N., Gueron, P., Bohlke-Schneider, M., and Wang, Y. Fev-bench: A realistic benchmark for time series forecasting. *arXiv preprint arXiv:2509.26468*, 2025.
- Shi, X., Wang, S., Nie, Y., Li, D., Ye, Z., Wen, Q., and Jin, M. Time-MoE: Billion-scale time series foundation models with mixture of experts. *Proceedings of the International Conference on Learning Representations*, 2025.
- Thomas, V., Ma, J., Hosseinzadeh, R., Golestan, K., Yu, G., Volkovs, M., and Caterini, A. Retrieval & fine-tuning for in-context tabular models. *Advances in Neural Information Processing Systems*, 37:108439–108467, 2024.
- Vaswani, A., Shazeer, N., Parmar, N., Uszkoreit, J., Jones, L., Gomez, A. N., Kaiser, Ł., and Polosukhin, I. Attention is all you need. *Advances in Neural Information Processing Systems*, 30, 2017.
- Wang, S., Li, C., and Lim, A. A model for non-stationary time series and its applications in filtering and anomaly detection. *IEEE Transactions on Instrumentation and Measurement*, 70:1–11, 2021.
- Wang, S., Wu, H., Shi, X., Hu, T., Luo, H., Ma, L., Zhang, J. Y., and Zhou, J. TimeMixer: Decomposable multiscale mixing for time series forecasting. In *Proceedings of the International Conference on Learning Representations*, 2024a.
- Wang, X., Zhou, T., Wen, Q., Gao, J., Ding, B., and Jin, R. CARD: Channel aligned robust blend transformer for time series forecasting. In *Proceedings of the International Conference on Learning Representations*, 2024b.
- Woo, G., Liu, C., Kumar, A., Xiong, C., Savarese, S., and Sahoo, D. Unified training of universal time series forecasting transformers. In *Proceedings of the International Conference on Machine Learning*, 2024.
- Wu, H., Xu, J., Wang, J., and Long, M. Autoformer: Decomposition transformers with auto-correlation for long-term series forecasting. *Advances in Neural Information Processing Systems*, 34:22419–22430, 2021.
- Xu, D., Cirit, O., Asadi, R., Sun, Y., and Wang, W. Mixture of in-context prompts for tabular PFNs. *Proceedings of the International Conference on Learning Representations*, 2025.
- Zhou, T., Ma, Z., Wen, Q., Sun, L., Yao, T., Yin, W., Jin, R., et al. Film: Frequency improved legendre memory model for long-term time series forecasting. *Advances in Neural Information Processing Systems*, 35:12677–12690, 2022a.
- Zhou, T., Ma, Z., Wen, Q., Wang, X., Sun, L., and Jin, R. FEDformer: Frequency enhanced decomposed transformer for long-term series forecasting. In *Proceedings of the International Conference on Machine Learning*, 2022b.

Zhou, T., Niu, P., Sun, L., Jin, R., et al. One fits all: Power general time series analysis by pretrained LM. *Advances in Neural Information Processing Systems*, 36:43322–43355, 2023.

Zhu, B., Shi, X., Erickson, N., Li, M., Karypis, G., and Shoaran, M. Xtab: Cross-table pretraining for tabular transformers. In *Proceedings of the International Conference on Machine Learning*, 2023.

## A. Implement details

### A.1. Model Details

Baguan-TS uses a 3D Transformer-based architecture with hyperparameters summarized in Table 6. The model has 22.4 million parameters.

Table 6. Baguan-TS model architecture hyperparameters.

Parameter	Value
Temporal patch size ( $P$ )	8
Number of 3D Transformer blocks ( $L$ )	12
Number of heads	6
Embedding dimension ( $D$ )	192
Feed-forward dimension	768
Output dimension ( $K$ )	5000

During training,  $C$ ,  $T$ ,  $H$ , and  $M$  are randomly sampled for each batch, up to fixed maximum values. We set  $C_{\max} = 50$  for the contexts,  $T_{\max} = 2048$  for the lookback length,  $H_{\max} = 192$  for the prediction horizon, and  $M_{\max} = 80$  for the number of covariates.

### A.2. Training Data

Training data is critical to the performance of a foundation model. Baguan-TS is trained on a mixture of synthetic data and real-world benchmark data. The real-world data provide grounding in practical distributions and noise characteristics, while the synthetic data are designed to span a broad family of dynamics, covariate roles, and latent-factor structures that are hard to obtain exhaustively from any single corpus.

**Synthetic Data.** The diverse and task-specific semantics of covariates in different forecasting tasks make it difficult to handcraft a single, general-purpose synthetic data simulator. Our key idea is that many covariate-aware forecasting problems can be viewed as regression with partially observed, time-correlated latent factors. Observed covariates are noisy or incomplete proxies for these latent drivers, while the target series combines autoregressive structure with nonlinear effects of both observed and latent inputs. Accordingly, we build a generic generator in which latent trajectories are drawn from a kernel dictionary, and transformed through a dynamic structural causal mechanism with a random MLP to induce nonlinear interactions. Only a subset of nodes is exposed as observed covariates and the remainder act as unobserved drivers; process and measurement noise, as well as optional regime shifts, are added to simulate different data characteristics. Within each task, the mechanism (graph, MLP weights, kernels, noise scales, exposure set) is fixed, whereas context and target instances draw independent latent realizations.

**Real-World Data.** We include the GIFT-Eval pretraining corpus (Aksu et al., 2024) in our training set and augment each time step with a time index feature. To simulate distribution shifts and expose the model to regime changes, we concatenate multiple normalized series into longer sequences and randomly sample contiguous subsequences as training examples.

### A.3. Training Loss

We use the continuous ranked probability score (CRPS) as the training loss. For a predictive CDF  $F$  and observation  $y$ ,  $\text{CRPS}(F, y) = \int_{-\infty}^{\infty} (F(z) - \mathbb{I}(z \geq y))^2 dz$ . When the predictive distribution is represented by  $K$  bins with centers  $h_i$ , we collect the probabilities into a vector  $\mathbf{p} = (p_1, \dots, p_K)^\top \in \mathbb{R}^K$  with  $\sum_i p_i = 1$ , the corresponding discrete form of each time step is

$$\text{CRPS} = \sum_{i=1}^K p_i |h_i - y| - \frac{1}{2} \sum_{i=1}^K \sum_{j=1}^K p_i p_j |h_i - h_j|, \quad (1)$$

where the first term is the expected absolute error under the forecast and the second term equals half the expected pairwise absolute distance between two independent forecast draws, acting as a sharpness term that discourages over-dispersion while preserving propriety. We compute CRPS per horizon step and average across the forecast window.

#### A.4. Inference Details

For the inference process, we implement a stochastic ensemble approach to enhance prediction robustness through input perturbation and multiple forward passes. Specifically, covariate column positions are randomly shuffled, and 20% of historical target values are masked during each inference iteration, with 2–4 independent forward passes performed. The output is the average of these forward passes.

In our experimental framework, a validation set is constructed for each time series by rolling the historical window backward by either 2 or 5 steps to simulate realistic forecasting conditions. The final predictions represent an ensemble of 2–9 distinct configurations selected based on their performance on this validation set. These configurations vary across four critical dimensions:

- Inference mode (2D/3D/2D+3D ensemble);
- Whether to include time series order, a blank column, or calendar-specific temporal features (e.g., year, month, day);
- Whether to apply reversible instance normalization (RevIn) (Kim et al., 2022) to each organized context;
- Context window length ( $T$ ), defined as an integer multiple of the prediction horizon, taking values from 2 to 14.

This ensemble strategy enhances architectural diversity, automatically addresses covariate-agnostic scenarios by prioritizing temporal pattern extraction, and mitigates the uncertainty caused by the changeable context length and RBfsc module.

## B. Details of Ablation Study

### B.1. Effect of 3D and 2D Ensemble

**Residual Analysis for Point Prediction.** We analyze the residual correlation between the 2D and 3D inference modes across all 30 covariate-aware tasks in the `fev-bench` dataset. The per-task Pearson correlation ranges from 0.42 to 0.95, with an aggregated value of 0.75 (Fig. 10a). The aggregated joint residual distribution is shown in Fig. 12c, revealing diverse error patterns that further support the effectiveness of combining 2D and 3D inference modes.

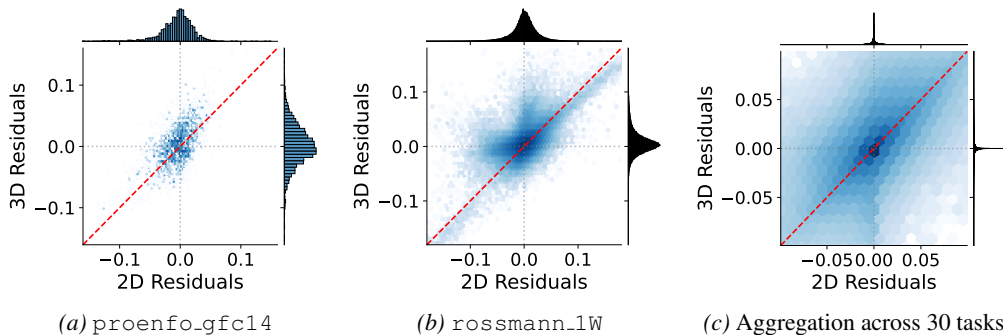


Figure 12. Joint residual distributions for the energy task `proenfo_gfc14`, the retail task `rossmann_1W`, and the aggregated results across all 30 tasks. Darker blue bins indicate higher data density. Points lying along the red dashed identity line ( $y = x$ ) correspond to instances where prediction errors are equal in both modes. Deviations from this diagonal, particularly in the second and fourth quadrants, reveal complementary error patterns between the two modes.

**Calibration Analysis for Probabilistic Analysis.** To assess the effectiveness and complementarity of the 2D and 3D inference modes, we analyze their probabilistic calibration. We compute histograms of the ground-truth quantile levels, also known as Probability Integral Transform (PIT) histograms. Specifically, for each observation  $y_t$  and predicted CDF  $\hat{F}_t$ , the quantile level is given by  $u_t = \hat{F}_t(y_t)$ . The x-axis represents these quantile levels ranging from 0 to 1, while the y-axis (labeled “Frequency”) indicates the relative frequency of ground truths falling into each quantile bin. A perfectly calibrated model should yield a uniform distribution, visualized as a flat line at Frequency = 0.1.

As shown in Figs. 13–15, the 2D and 3D modes exhibit diverse error structures across different tasks. On the `epf_de` task (Fig. 13), the 2D mode shows a distinct decreasing trend, indicating a systematic positive bias (over-estimation), as ground

truths frequently fall into lower quantiles. Conversely, the 3D mode displays an increasing trend, indicating a negative bias. These opposing biases effectively cancel out in the ensemble mode, resulting in a well-calibrated histogram. On the `hermes` task (Fig. 14), the 2D mode shows a U-shaped distribution, indicating over-confident predictions. In contrast, the 3D mode demonstrates superior calibration performance. Aggregated across all tasks (Fig. 15), the 2D mode consistently exhibits a U-shaped pattern, reflecting overconfident predictions with under-dispersed distributions, whereas the 3D mode maintains more stable calibration performance with slight under-confidence. The ensemble strategy effectively mitigates their weaknesses, resulting in robust probabilistic performance.

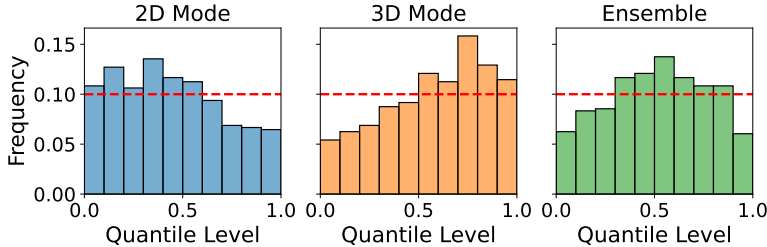


Figure 13. Calibration histograms of ground-truth quantile levels in predicted CDFs for different inference modes on `epf_de` (energy task).

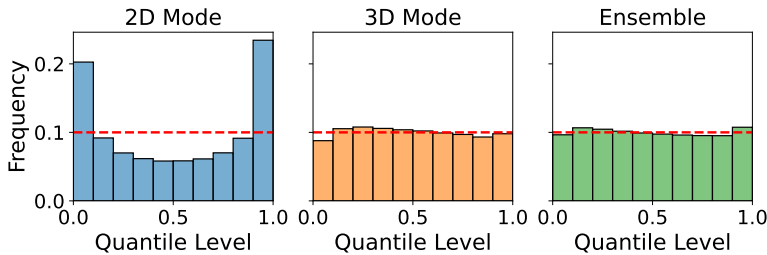


Figure 14. Calibration histograms of ground-truth quantile levels in predicted CDFs for different inference modes on `hermes` (retail task).

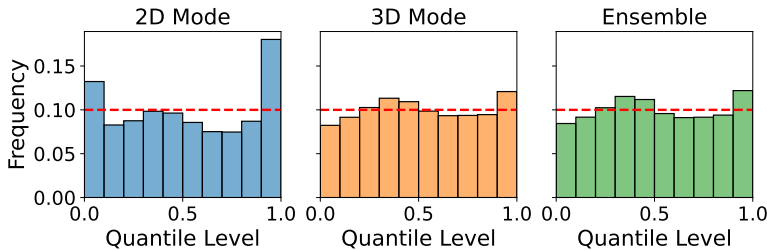


Figure 15. Calibration histograms of ground-truth quantile levels in predicted CDFs for different inference modes on `fev-bench-cov` dataset (across all 30 tasks).

### B.2. Robustness to Injected Noise

To more rigorously evaluate the robustness and stability of the proposed local calibration module, we conduct a noise injection experiment on the `epf_fr` dataset. Specifically, we corrupt the original time series with three types of synthetic stochastic noise: Gaussian white noise, random walk noise, and periodic noise (Chang, 2010; Kim & Chung, 2024; Wang et al., 2021). For each noise type, the intensity is controlled by a scaling factor  $\kappa \in \{0.05, 0.1, 0.2, 0.4, 0.6, 0.8, 1.0\}$ . The actual scale parameter used is defined as  $\sigma \cdot \kappa$ , where  $\sigma$  denotes the empirical standard deviation of the original time series.

For Gaussian white noise, we sample independent and identically distributed (i.i.d.) values from a normal distribution  $\mathcal{N}(0, \sigma\kappa)$  to obtain uncorrelated perturbations that mimic stationary noise.

For random walk noise, inspired by (Wang et al., 2021), we aim to mimic non-stationary noise with a directional trend. We first generate i.i.d. Gaussian increments  $\epsilon_t \sim \mathcal{N}(0, \sigma\kappa)$  and then compute their cumulative sum to form a random walk process:  $w_t = \sum_{i=1}^t \epsilon_i$ . This introduces temporally correlated perturbations and can simulate accumulated uncertainty over time.

Finally, we introduce periodic noise (Chang, 2010) to mimic seasonal interference using a sinusoidal signal with random frequency and phase:

$$p_t^{\text{noise}} = (\sigma\kappa) \cdot \sin\left(\frac{2\pi t}{T} + \phi\right),$$

where the period  $T$  is uniformly sampled from the interval  $[12, 60]$  to emulate diverse seasonal patterns (e.g., daily or weekly cycles), and the phase offset  $\phi$  is drawn uniformly from  $[0, 2\pi)$ . To avoid overly idealized waveforms, we further add a small amount of Gaussian background noise with standard deviation  $0.1 \cdot \sigma\kappa$ .

We report results based on a single forward pass without any ensemble strategy for our method, and use `n_estimators = 2` for TabPFN-TS, with a context length of 50,000 and the full set of clean running index and calendar features. The results are shown in Fig. 8. Our approaches—especially Y-space RBfct—maintain stronger robustness than TabPFN-TS across all noise types and intensities.

### B.3. Context-Overfitting on Synthetic Data

To simulate controllable periodic spikes, we formulate a synthetic time series using  $f(t) = \exp(k \cdot (\sin(\frac{2\pi t}{50}) - 1))$  (see Fig. 16). The spike sharpness is controlled by the parameter  $k$ , with larger values of  $k$  producing sharper spikes.

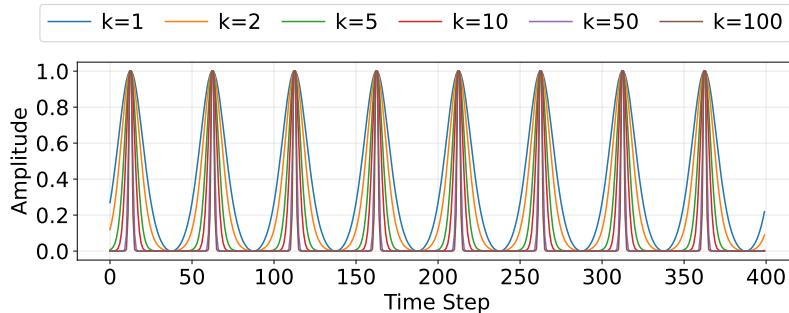


Figure 16. Toy periodic spike data generated using  $f(t) = \exp(k \cdot (\sin(\frac{2\pi t}{50}) - 1))$ . A larger  $k$  value results in a sharper periodic spike signal.

As shown in Fig. 17, distinct attention patterns emerge between the context-overfitting model and the baseline. At the peak prediction step (Figs. 17a and 17c), the attention weights of the context-overfitting model precisely align with the historical peak points within the lookback window. In contrast, the baseline model exhibits a diffuse attention distribution with a noticeable magnitude drop at these critical peak positions.

For the trough prediction in the flat region (Figs. 17b and 17d), the context-overfitting model shows more precise attention behavior. In the penultimate layer, the context-overfitting model effectively attends to the target flat region, aligning closely with the ground-truth dynamics. By the final layer, it manifests a dual-focus strategy, aggregating information from both historical peaks and target flat regions, which likely combines both global periodicity and local context to refine the final prediction. Conversely, the baseline model shows a more diffuse and scattered attention pattern across these two layers. It generates more uniform attention over the flat parts and displays a symmetric pattern around the peaks, lacking the precise localization ability found in the context-overfitting model. Overall, this comparison suggests that the context-overfitting approach learns a sharper, structure-aware representation of time series.

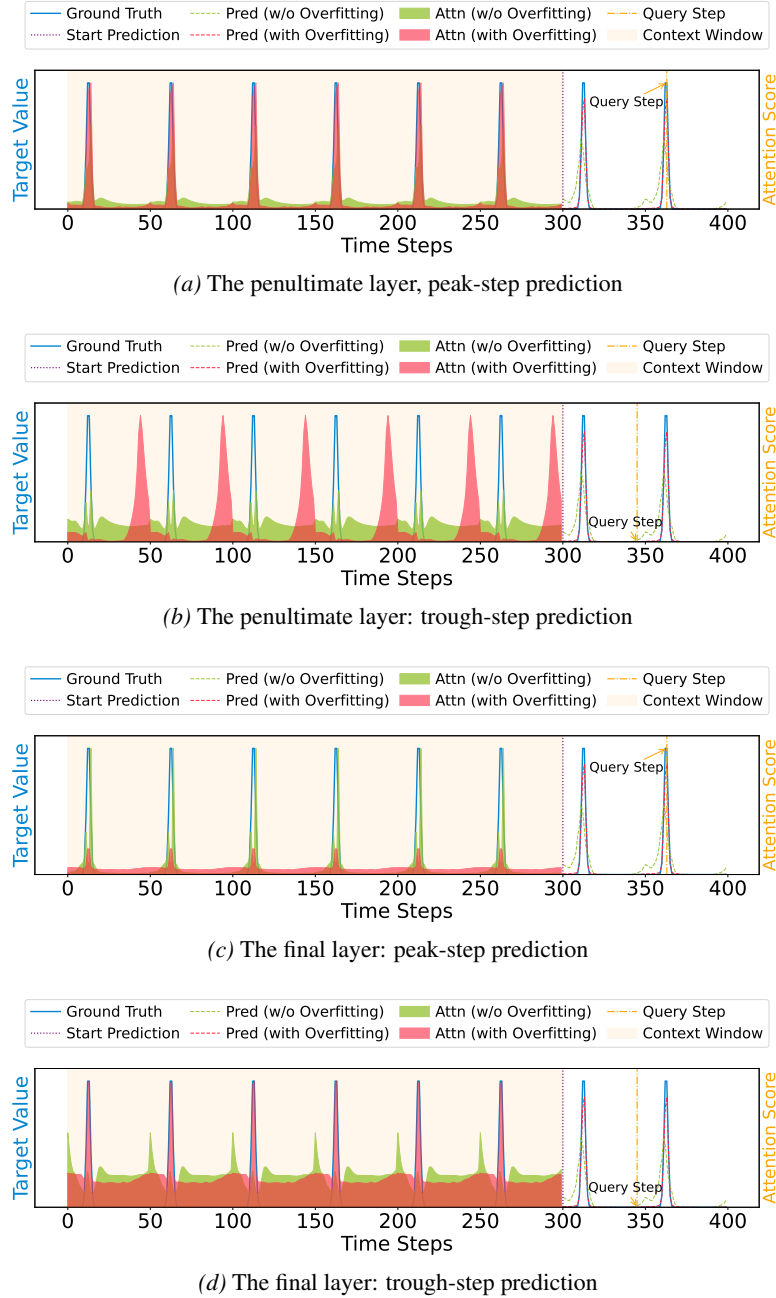


Figure 17. Attention weight maps on the synthetic spike series for the baseline model (w/o overfitting) and the context-overfitting model (with overfitting). Each subplot overlays the ground-truth signal, model predictions, and the corresponding attention distribution within the context window at the query step (orange dash-dot line).

## C. Detailed Experimental Results

### C.1. Results on Covariate-Aware Tasks

We provide detailed descriptions in Table 7 of the 30 covariate-aware forecasting tasks selected from `fev-bench`, which we denote as `fev-bench-cov`. The average skill scores across all evaluation metrics (SQL, MASE, WAPE, and WQL) are shown in Figs. 18–20. Our model attains either the best or second-best skill score on all four metrics, consistently outperforming other covariate-aware time series foundation models, such as TabPFN-TS. The detailed experimental results for each task are presented in Tables 8–16. Results for our method employ the ensemble strategy described in Appendix A.4;

baseline results are sourced from the official `fev-bench` benchmark.

To further assess performance in covariate-rich settings, we also include 27 proprietary real-world datasets from production: 18 city-level electricity load datasets and 9 city-level distributional photovoltaic (PV) generation forecasting tasks, all collected from different cities in China. To mirror real deployments, these 27 datasets include the full set of production covariates, notably numerical weather prediction (NWP) features and calendar effects. Table 17 reports the average performance across these 27 datasets. Baguan-TS achieves the best overall results on all four evaluation metrics, demonstrating strong performance in practical, covariate-rich forecasting settings.

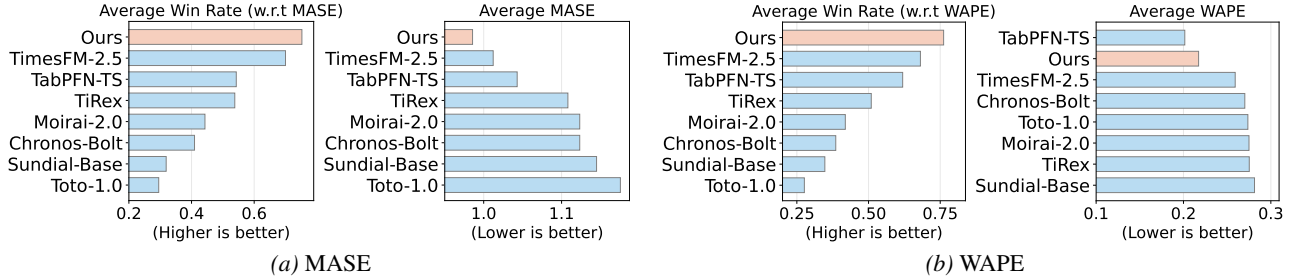


Figure 18. Point forecasting evaluation on `fev-bench-cov`.

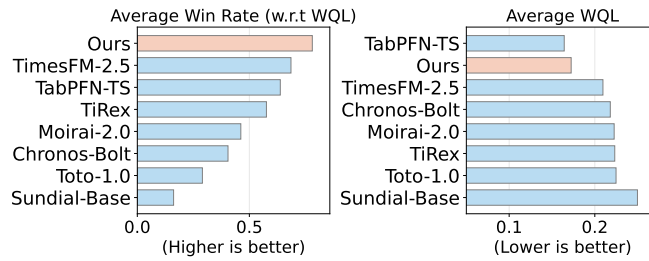


Figure 19. Probabilistic forecasting evaluation on `fev-bench-cov` using WQL.

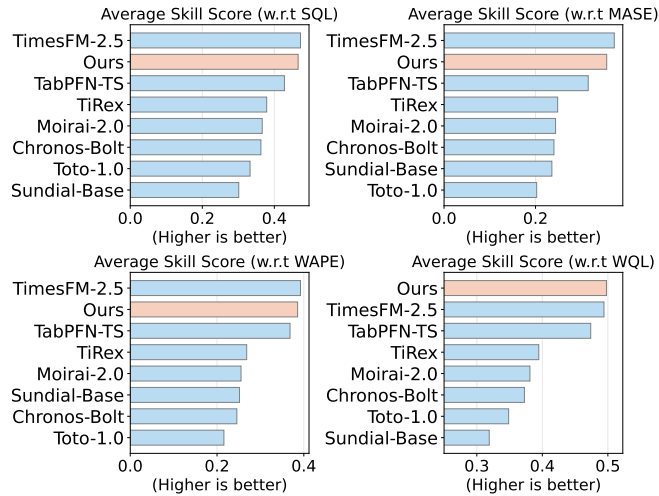


Figure 20. Skill score comparison on `fev-bench-cov`, using Seasonal Naive as the baseline model.

### C.2. Results on Univariate Tasks

We provide detailed information in Table 18 for the 10 univariate and multivariate forecasting tasks selected from `fev-bench-mini`, which we denote as `fev-bench-uni`. The corresponding ranking results, evaluated by macro-averaged SQL, MASE, WAPE, and WQL across these 10 datasets, are presented in Table 19. While adapting our 3D model

Table 7. Detailed overview of the 30 covariate-aware tasks from the fev-bench benchmark, collectively referred to as fev-bench-cov.

Task	Domain	Frequency	# items	median length	# obs	# known dynamic cols	H	W	# seasonality	# targets
entsoe_15T	energy	15 Min	6	175,292	6,310,512	3	96	20	96	1
entsoe_1H	energy	1 H	6	43,822	1,577,592	3	96	20	48	1
entsoe_30T	energy	30 Min	6	87,645	3,155,220	3	168	20	24	1
epf_be	energy	1 H	1	52,416	157,248	2	24	20	24	1
epf_de	energy	1 H	1	52,416	157,248	2	24	20	24	1
epf_fr	energy	1 H	1	52,416	157,248	2	24	20	24	1
epf_np	energy	1 H	1	52,416	157,248	2	24	20	24	1
epf_pjm	energy	1 H	1	52,416	157,248	2	24	20	24	1
proenfo_gfc12	energy	1 H	11	39,414	867,108	1	168	10	24	1
proenfo_gfc14	energy	1 H	1	17,520	35,040	1	168	20	24	1
proenfo_gfc17	energy	1 H	8	17,544	280,704	1	168	20	24	1
solar_with_weather_15T	energy	15 Min	1	198,600	1,986,000	7	96	20	96	1
solar_with_weather_1H	energy	1 H	1	49,648	496,480	7	24	20	24	1
uci_air_quality_1D	nature	Daily	1	389	5,057	3	28	11	7	4
uci_air_quality_1H	nature	1 H	1	9,357	121,641	3	168	20	24	4
m5_1D	retail	Daily	30,490	1,810	428,849,460	8	28	1	7	1
m5_1M	retail	Monthly	30,490	58	13,805,685	8	12	1	12	1
m5_1W	retail	Weekly	30,490	257	60,857,703	8	13	1	1	1
rohlik_orders_1D	retail	Daily	7	1,197	115,650	4	61	5	7	1
rohlik_orders_1W	retail	Weekly	7	170	15,316	4	8	5	1	1
rohlik_sales_1D	retail	Daily	5,390	1,046	74,413,935	13	14	1	7	1
rohlik_sales_1W	retail	Weekly	5,243	150	10,516,770	13	8	1	1	1
rossmann_1D	retail	Daily	1,115	942	7,352,310	5	48	10	7	1
rossmann_1W	retail	Weekly	1,115	133	889,770	4	13	8	1	1
walmart	retail	Weekly	2,936	143	4,609,143	10	39	1	1	1
hermes	retail	Weekly	10,000	261	5,220,000	1	52	1	1	1
favorita_stores_1D	retail	Daily	1,579	1,688	10,661,408	2	28	10	7	1
favorita_stores_1M	retail	Monthly	1,579	54	255,798	1	12	2	12	1
favorita_stores_1W	retail	Weekly	1,579	240	1,136,880	1	13	10	1	1
favorita_transactions_1D	retail	Daily	51	1,688	258,264	1	28	10	7	1

Table 8. Performance Comparison on proenfo\_gfc12, proenfo\_gfc14, and proenfo\_gfc17. The best results are highlighted in bold, and the second-best results are underlined.

Model	gfc12				gfc14				gfc17			
	SQL	MASE	WAPE	WQL	SQL	MASE	WAPE	WQL	SQL	MASE	WAPE	WQL
AutoARIMA	1.1408	1.3848	0.1193	0.0987	0.9471	1.1681	0.0571	0.0464	1.1150	1.3821	0.0943	0.0762
AutoETS	2.4309	2.8114	0.2331	0.2073	1.1104	1.3186	0.0647	0.0545	2.1346	2.4128	0.1663	0.1466
AutoTheta	1.4149	1.5237	0.1360	0.1251	1.0555	1.1857	0.0580	0.0519	1.1470	1.3687	0.0931	0.0770
Chronos-Bolt	0.9172	1.0781	0.0910	0.0773	0.7674	0.9285	0.0455	0.0376	0.9004	1.0977	0.0745	0.0608
Moirai-2.0	0.7928	0.9538	0.0803	0.0668	0.6766	0.8458	0.0413	0.0330	0.7740	0.9628	0.0647	0.0519
Naive	2.3796	2.6291	0.2326	0.2075	3.2096	3.7073	0.1831	0.1588	2.5750	2.9066	0.1911	0.1691
Seasonal Naive	1.1997	1.4282	0.1285	0.1088	1.0751	1.1989	0.0587	0.0529	1.3160	1.5845	0.1078	0.0897
Stat. Ensemble	1.3049	1.5463	0.1407	0.1182	0.9059	1.1044	0.0540	0.0444	1.1417	1.4215	0.0960	0.0770
Sundial-Base	0.9004	0.9936	0.0814	0.0733	<u>0.4208</u>	<u>0.4636</u>	<u>0.0226</u>	<u>0.0205</u>	<u>0.5086</u>	<u>0.5526</u>	<u>0.0343</u>	<u>0.0316</u>
TabPFN-TS	0.8345	1.0338	0.0878	0.0702	0.5148	0.6406	0.0314	0.0252	0.6717	0.8553	0.0563	0.0441
TimesFM-2.5	<b>0.1876</b>	<b>0.2168</b>	<b>0.0163</b>	<b>0.0143</b>	<b>0.1403</b>	<b>0.1688</b>	<b>0.0083</b>	<b>0.0069</b>	<b>0.1601</b>	<b>0.1898</b>	<b>0.0120</b>	<b>0.0101</b>
TiRex	0.9081	1.1242	0.0954	0.0771	0.7206	0.9119	0.0447	0.0354	0.8894	1.1381	0.0764	0.0597
Toto-1.0	0.9344	1.1371	0.0972	0.0795	0.7346	0.9215	0.0452	0.0360	0.9388	1.1961	0.0799	0.0626
Ours	<u>0.6646</u>	<u>0.8282</u>	<u>0.0691</u>	<u>0.0554</u>	0.4628	0.5772	0.0284	0.0227	0.5239	0.6642	0.0432	0.0341

Table 9. Performance Comparison on rohlik\_sales\_1D, rohlik\_orders\_1D, rohlik\_sales\_1W, and rohlik\_orders\_1W. The best results are highlighted in **bold**, and the second-best results are underlined.

Model	sales_1D				orders_1D				sales_1W				orders_1W			
	SQL	MASE	WAPE	WQL												
AutoARIMA	1.2758	1.5092	0.4095	0.3459	1.2662	1.5624	0.0741	0.0604	1.8025	2.0379	0.3070	0.2670	1.4147	1.7324	0.0584	0.0471
AutoETS	1.2662	1.4986	0.4185	0.3543	1.4470	1.4870	0.0657	0.0637	14.4532	1.8900	0.3003	4.0491	1.4190	1.7583	0.0582	0.0469
AutoTheta	1.2818	1.4939	0.4131	0.3563	1.3973	1.5185	0.0664	0.0607	1.6547	1.8364	0.2946	0.2656	1.3963	1.7122	0.0573	0.0465
Chronos-Bolt	1.1471	1.3871	0.3783	0.3140	1.0508	1.3016	0.0614	0.0495	1.5216	1.8467	0.2846	0.2337	1.4282	1.7219	0.0570	0.0471
Moirai-2.0	1.1696	1.4021	0.3821	0.3202	<b>0.9700</b>	<b>1.1761</b>	<b>0.0552</b>	<b>0.0455</b>	1.5157	1.8215	0.2871	0.2365	1.5315	1.8740	0.0612	0.0501
Naive	1.5460	1.7485	0.4717	0.4099	2.9130	2.4354	0.1083	0.1384	1.9282	1.9155	0.3119	0.3323	1.4844	1.7312	0.0584	0.0499
Seasonal Naive	1.3750	1.6150	0.4346	0.3728	1.5544	1.7783	0.0827	0.0730	1.9282	1.9155	0.3119	0.3323	1.4844	1.7312	0.0584	0.0499
Stat. Ensemble	1.2483	1.4760	0.4057	0.3425	1.2114	1.3812	0.0628	0.0552	1.6455	1.8250	0.2906	0.2596	1.3984	1.7128	0.0573	0.0465
Sundial-Base	1.2027	1.3443	0.3645	0.3250	1.1963	1.3993	0.0667	0.0571	1.6933	1.8996	0.2929	0.2594	1.8923	2.0952	0.0675	0.0609
TabPFN-TS	-	-	-	-	1.3411	1.5479	0.0656	0.0585	<u>1.2205</u>	<u>1.5205</u>	<u>0.2152</u>	<u>0.1698</u>	1.5240	1.9887	0.0652	0.0500
TimesFM-2.5	<u>1.0958</u>	<u>1.3238</u>	<u>0.3586</u>	<u>0.2984</u>	1.0057	1.2504	0.0591	0.0473	1.4010	1.6891	0.2667	0.2197	<u>1.3278</u>	<u>1.6592</u>	<u>0.0542</u>	<u>0.0430</u>
TiRex	1.1481	1.3845	0.3784	0.3154	<u>0.9858</u>	<u>1.2034</u>	<u>0.0572</u>	<u>0.0468</u>	1.4252	1.7354	0.2736	0.2252	<b>1.3004</b>	<b>1.5829</b>	<b>0.0521</b>	<b>0.0426</b>
Toto-1.0	1.2181	1.4539	0.3975	0.3352	1.1351	1.3776	0.0646	0.0532	1.5046	1.8031	0.2812	0.2348	1.4934	1.7980	0.0591	0.0489
Ours	<b>0.8725</b>	<b>1.0930</b>	<b>0.2663</b>	<b>0.2114</b>	1.1684	1.4377	0.0669	0.0546	<b>1.1827</b>	<b>1.4646</b>	<b>0.2045</b>	<b>0.1627</b>	1.5405	1.8940	0.0608	0.0493

Table 10. Performance Comparison on entsoe\_15T, entsoe\_30T, and entsoe\_1H. The best results are highlighted in **bold**, and the second-best results are underlined.

Model	15T				30T				1H			
	SQL	MASE	WAPE	WQL	SQL	MASE	WAPE	WQL	SQL	MASE	WAPE	WQL
AutoARIMA	—	—	—	—	0.9807	1.2299	0.0909	0.0732	0.8725	1.1176	0.0854	0.0667
AutoETS	3.0289	4.0070	0.4081	0.3140	2.4928	3.2738	0.2412	0.1816	1.9050	2.0475	0.1570	0.1447
AutoTheta	0.5794	0.7298	0.0540	0.0430	0.7997	1.0040	0.0721	0.0572	0.9723	1.1626	0.0836	0.0694
Chronos-Bolt	0.5062	0.6062	0.0428	0.0363	0.5294	0.6326	<u>0.0378</u>	0.0321	0.4574	0.5564	0.0341	0.0282
Moirai-2.0	0.4783	<u>0.5933</u>	0.0424	0.0343	<u>0.4884</u>	<u>0.5974</u>	0.0383	0.0318	0.4871	0.5924	0.0396	0.0333
Naive	1.5177	1.9046	0.1434	0.1155	1.6092	2.0733	0.1463	0.1142	1.9154	2.0553	0.1571	0.1448
Seasonal Naive	0.7807	0.9315	0.0677	0.0566	1.0103	1.2162	0.0871	0.0726	1.0561	1.1015	0.0792	0.0798
Stat. Ensemble	—	—	—	—	0.8465	1.0578	0.0767	0.0612	0.8920	1.1145	0.0833	0.0660
Sundial-Base	0.6669	0.7578	0.0565	0.0500	0.7216	0.7796	0.0520	0.0486	0.7441	0.8118	0.0555	0.0510
TabPFN-TS	0.4837	0.6094	0.0426	<b>0.0335</b>	0.5117	0.6350	0.0391	0.0322	<u>0.4419</u>	<u>0.5377</u>	<u>0.0333</u>	<u>0.0273</u>
TimesFM-2.5	<u>0.4709</u>	<b>0.5903</b>	<b>0.0416</b>	<b>0.0335</b>	0.5658	0.6958	0.0473	0.0388	0.4681	0.5849	0.0359	0.0290
TiRex	<b>0.4693</b>	0.5986	<u>0.0420</u>	<u>0.0337</u>	0.5230	0.6646	0.0400	0.0314	0.4701	0.5854	0.0363	0.0294
Toto-1.0	0.5909	0.7503	0.0523	0.0414	0.4958	0.6254	0.0379	<u>0.0302</u>	0.4796	0.5908	0.0366	0.0302
Ours	0.5261	0.6586	0.0458	0.0366	<b>0.4441</b>	<b>0.5538</b>	<b>0.0365</b>	<b>0.0295</b>	<b>0.3859</b>	<b>0.4819</b>	<b>0.0287</b>	<b>0.0231</b>

Table 11. Performance Comparison on epf\_be, epf\_de, epf\_fr, epf\_np, and epf\_pjm. The best results are highlighted in **bold**, and the second-best results are underlined.

Model	be				de				fr				np				pjm			
	SQL	MASE	WAPE	WQL																
AutoARIMA	1.0561	1.0948	0.1986	0.1868	1.2777	1.6231	0.6819	0.5433	1.1581	0.9888	0.1532	0.1715	1.3932	1.7096	0.0786	0.0637	0.4819	0.5573	0.0985	0.0855
AutoETS	1.5343	1.3929	0.2488	0.2659	1.4013	1.7417	0.6107	0.5288	0.8989	0.9665	0.1493	0.1387	1.9332	2.3244	0.1041	0.0864	0.9139	0.9847	0.1717	0.1607
AutoTheta	1.4843	1.0194	0.1882	0.2582	1.4944	1.4072	0.6460	0.6490	1.5912	0.8447	0.1294	0.2296	1.2812	1.5140	0.0688	0.0579	0.6032	0.6832	0.1199	0.1068
Chronos-Bolt	0.5731	0.7273	0.1357	0.1069	1.0208	1.2655	0.5607	0.4644	0.4389	0.5638	0.0877	0.0685	0.9711	1.2409	0.0567	0.0445	0.4217	0.5357	0.0938	0.0739
Moirai-2.0	0.5281	0.6709	0.1228	0.0968	1.0164	1.2282	0.5365	0.4586	0.4092	0.5035	0.0791	0.0646	0.9253	1.1998	0.0543	0.0420	0.4405	0.5631	0.0976	0.0766
Naive	3.0845	1.3609	0.2376	0.5357	1.4012	1.7417	0.6107	0.5287	3.8189	1.1603	0.1703	0.5501	1.9404	2.3155	0.1037	0.0869	0.9298	0.9849	0.1717	0.1642
Seasonal Naive	1.1503	1.0271	0.1840	0.2013	1.3877	1.7086	0.7490	0.5919	1.2455	0.8501	0.1298	0.1818	1.5298	1.7613	0.0796	0.0692	0.5153	0.5812	0.1016	0.0908
Stat. Ensemble	1.2135	0.9814	0.1754	0.2109	1.1666	1.3821	0.6023	0.4882	1.1456	0.7410	0.1133	0.1677	1.2844	1.5147	0.0683	0.0574	0.4871	0.5295	0.0934	0.0863
Sundial-Base	0.6465	0.7222	0.1303	0.1170	1.1831	1.3227	0.5722	0.5103	0.4611	0.5244	0.0813	0.0720	0.9451	1.0947	0.0496	0.0428	0.4679	0.5214	0.0934	0.0841
TabPFN-TS	0.5324	0.6702	0.1180	0.0933	<b>0.4403</b>	<b>0.5675</b>	<b>0.3069</b>	<b>0.2426</b>	<b>0.3307</b>	<b>0.4182</b>	<b>0.0618</b>	<b>0.0491</b>	<b>0.6593</b>	<b>0.8709</b>	<b>0.0387</b>	<b>0.0293</b>	0.4270	0.5340	0.0925	0.0740
TimesFM-2.5	<b>0.4937</b>	<b>0.6102</b>	<b>0.1126</b>	<b>0.0905</b>	1.0300	1.2799	0.5914	0.4775	0.4092	0.4907	0.0771	0.0640	1.1706	1.4402	0.0639	0.0519	0.4263	0.5311	0.0942	0.0757
TiRex	0.5270	0.6744	0.1230	0.0962	1.0322	1.2971	0.5787	0.4685	0.4014	0.5040	0.0798	0.0639	0.9662	1.2226	0.0554	0.0438	<u>0.4042</u>	<u>0.5058</u>	<u>0.0894</u>	<u>0.0714</u>
Toto-1.0	0.5648	0.7065	0.1323	0.1058	1.1058	1.3370	0.6772	0.5515	0.4257	0.5253	0.0837	0.0683	1.0369	1.3589	0.0616	0.0471	0.4519	0.5822	0.1031	0.0800
Ours	<u>0.5162</u>	<u>0.6550</u>	<u>0.1159</u>	<u>0.0908</u>	<u>0.4597</u>	<u>0.5882</u>	<u>0.3424</u>	<u>0.2525</u>	<u>0.3518</u>	<u>0.4517</u>	<u>0.0675</u>	<u>0.0529</u>	<u>0.7174</u>	<u>0.9241</u>	<u>0.0415</u>	<u>0.0321</u>	<b>0.3716</b>	<b>0.4603</b>	<b>0.0798</b>	<b>0.0646</b>

Table 12. Performance Comparison on rossmann\_1D, rossmann\_1W, hermes, and walmart. The best results are highlighted in **bold**, and the second-best results are underlined.

Model	rossmann_1D				rossmann_1W				hermes				walmart			
	SQL	MASE	WAPE	WQL												
AutoARIMA	0.5619	0.6544	0.2224	0.1908	0.5212	0.6689	0.1836	0.1410	1.2129	1.5317	0.0064	0.0050	1.0205	1.2474	0.1596	0.1320
AutoETS	0.5937	0.6913	0.2361	0.2028	0.5175	0.6685	0.1836	0.1402	1.6730	1.9852	0.0088	0.0074	-	1.7227	0.2951	-
AutoTheta	0.8315	0.7448	0.2558	0.2910	0.5160	0.6644	0.1813	0.1385	1.5539	1.8478	0.0081	0.0068	1.4675	1.4179	0.1852	0.1997
Chronos-Bolt	0.5246	0.6371	0.2176	0.1788	0.4871	0.6452	0.1760	0.1317	0.6752	0.8579	0.0032	0.0025	0.7740	0.9671	0.1173	0.0950
Moirai-2.0	0.5274	0.6480	0.2215	0.1799	0.4969	0.6440	0.1759	0.1342	0.7038	0.8854	0.0034	0.0027	0.8447	1.0559	0.1315	0.1058
Naive	2.7621	1.6195	0.5481	0.9389	0.8988	0.7960	0.2192	0.2509	2.1461	1.9945	0.0087	0.0087	2.0341	1.5241	0.1967	0.3075
Seasonal Naive	0.9137	0.7886	0.2692	0.3140	0.8988	0.7960	0.2192	0.2509	2.1461	1.9945	0.0087	0.0087	2.0341	1.5241	0.1967	0.3075
Stat. Ensemble	0.5781	0.6678	0.2278	0.1969	0.5014	0.6513	0.1783	0.1351	1.4162	1.8121	0.0079	0.0061	1.2166	1.3564	0.1773	0.1644
Sundial-Base	0.5306	0.6155	0.2092	0.1802	0.5781	0.6790	0.1855	0.1572	0.8243	0.9595	0.0037	0.0031	0.8422	0.9842	0.1211	0.1036
TabPFN-TS	<b>0.2321</b>	<b>0.2945</b>	<b>0.0979</b>	<b>0.0772</b>	<b>0.2539</b>	<b>0.3046</b>	<b>0.0792</b>	<b>0.0660</b>	0.7049	0.9123	0.0034	0.0026	<b>0.6619</b>	<b>0.8318</b>	<b>0.0943</b>	<b>0.0752</b>
TimesFM-2.5	0.5016	0.6106	0.2086	0.1711	0.4952	0.6543	0.1803	0.1351	<b>0.6184</b>	<b>0.7872</b>	<b>0.0029</b>	<b>0.0023</b>	<u>0.6794</u>	<u>0.8615</u>	<u>0.1016</u>	<u>0.0803</u>
TiRex	0.5391	0.6601	0.2251	0.1837	0.4816	0.6218	0.1697	0.1304	0.6510	0.8310	0.0031	<u>0.0024</u>	0.7075	0.8862	0.1054	0.0850
Toto-1.0	0.5677	0.6814	0.2321	0.1932	0.4944	0.6319	0.1733	0.1345	0.9853	1.2023	0.0044	0.0036	0.9072	1.1258	0.1385	0.1135
Ours	<u>0.2720</u>	<u>0.3348</u>	<u>0.1120</u>	<u>0.0910</u>	<u>0.2787</u>	<u>0.3371</u>	<u>0.0854</u>	<u>0.0705</u>	<u>0.6185</u>	<u>0.7971</u>	<u>0.0030</u>	<b>0.0023</b>	0.7621	1.0047	0.1305	0.0925

 Table 13. Performance Comparison on m5\_1D, m5\_1W, and m5\_1M. The best results are highlighted in **bold**, and the second-best results are underlined.

Model	1D				1W				1M			
	SQL	MASE	WAPE	WQL	SQL	MASE	WAPE	WQL	SQL	MASE	WAPE	WQL
AutoARIMA	0.8517	1.0631	0.7717	0.6115	0.9367	1.1568	0.4388	0.3580	1.0455	1.2131	0.4601	0.3801
AutoETS	0.8528	1.0633	0.7714	0.6156	0.9531	1.1672	0.4468	0.3728	1.1082	1.2139	0.4605	0.4321
AutoTheta	0.8721	1.0806	0.7779	0.6265	0.9634	1.1698	0.4475	0.3767	1.0987	1.2590	0.4910	0.4195
Chronos-Bolt	0.7293	0.8852	0.7110	0.5620	0.9165	1.1647	0.4334	0.3410	1.0001	1.1852	0.4455	0.3566
Moirai-2.0	<u>0.7096</u>	<u>0.8691</u>	<u>0.6984</u>	0.5508	0.9069	1.1501	0.4286	0.3361	0.9959	1.1773	0.4363	0.3457
Seasonal Naive	1.2545	1.2236	0.9159	0.8589	1.3558	1.3382	0.5042	0.5199	1.1399	1.3266	0.5108	0.4286
Sundial-Base	0.8516	0.9678	0.7357	0.6370	0.9748	1.1331	0.4258	0.3623	1.0815	1.1996	0.4509	0.3886
TabPFN-TS	-	-	-	-	0.9282	1.1605	0.4358	0.3437	1.0017	1.1871	0.4365	0.3467
TimesFM-2.5	0.7189	0.8721	<b>0.6968</b>	<u>0.5507</u>	<b>0.8890</b>	<u>1.1222</u>	<b>0.4201</b>	<b>0.3312</b>	<u>0.9798</u>	<b>1.1576</b>	<u>0.4249</u>	<b>0.3370</b>
TiRex	0.7144	0.8753	0.7025	0.5523	0.9026	1.1477	0.4281	0.3359	<b>0.9740</b>	1.1629	0.4306	<u>0.3447</u>
Toto-1.0	<b>0.7076</b>	<b>0.8683</b>	0.6986	<b>0.5495</b>	0.9050	1.1448	0.4278	0.3369	1.0440	1.2422	0.4597	0.3648
Ours	0.7235	1.0231	0.7461	0.5524	<u>0.9011</u>	<b>1.1221</b>	<u>0.4214</u>	<u>0.3319</u>	1.0080	<u>1.1581</u>	<b>0.4240</b>	0.3462

 Table 14. Performance Comparison on favorita\_stores (1D/1W/1M) and favorita\_transactions\_1D. The best results are highlighted in **bold**, and the second-best results are underlined.

Model	stores_1D				stores_1W				stores_1M				transactions_1D			
	SQL	MASE	WAPE	WQL	SQL	MASE	WAPE	WQL	SQL	MASE	WAPE	WQL	SQL	MASE	WAPE	WQL
AutoARIMA	1.2216	1.4188	0.1934	0.1647	2.2969	2.5801	0.1501	0.1331	2.0382	2.2075	0.1385	0.1314	1.5622	1.7409	0.1205	0.1055
AutoETS	1.2379	1.3799	0.1872	0.1672	2.3568	2.5165	0.1484	0.1430	1.9424	2.1221	0.1568	0.1329	1.1813	1.2765	0.1010	0.0945
AutoTheta	1.2732	1.3759	0.1835	0.1779	2.3160	2.4768	0.1444	0.1408	1.9416	2.1335	0.1535	0.1245	1.2463	1.2511	0.0961	0.0991
Chronos-Bolt	1.0322	1.2689	0.1743	0.1419	2.1011	2.4749	0.1580	0.1268	2.0865	2.4178	0.2637	0.1852	<u>0.9750</u>	<u>1.1515</u>	0.0873	0.0736
Moirai-2.0	0.9798	1.2047	0.1568	0.1279	2.1965	2.5773	0.1555	0.1243	2.0913	2.3236	0.2355	0.1726	1.1211	1.3295	0.0837	0.0705
Naive	2.6357	1.8830	0.3056	0.4079	2.4938	2.5171	0.1528	0.1608	2.0578	<b>1.9974</b>	<u>0.1233</u>	0.1701	2.7304	1.8618	0.1561	0.2372
Seasonal Naive	1.6902	1.7590	0.2520	0.2376	2.4938	2.5171	0.1528	0.1608	2.0967	2.2823	0.1900	0.1715	1.7338	1.8200	0.1461	0.1403
Stat. Ensemble	1.1971	1.3400	0.1789	0.1606	2.2196	2.4340	0.1436	0.1336	1.9426	<u>2.1181</u>	0.1467	0.1265	1.1848	1.2658	0.1005	0.0949
Sundial-Base	1.0613	1.2200	0.1562	0.1354	2.3082	2.5612	0.1497	0.1312	2.2543	2.4060	0.2561	0.2222	1.1982	1.3247	0.0799	0.0711
TabPFN-TS	0.9698	1.1943	<u>0.1486</u>	<u>0.1204</u>	2.1227	2.5268	<u>0.1260</u>	<u>0.1011</u>	<u>1.9336</u>	2.1758	<b>0.1159</b>	<b>0.0943</b>	1.2252	1.6727	<u>0.0773</u>	<u>0.0603</u>
TimesFM-2.5	<b>0.9494</b>	<b>1.1676</b>	<b>0.1452</b>	<b>0.1184</b>	<b>1.9684</b>	<b>2.2901</b>	0.1308	0.1095	1.9983	2.2338	0.2103	0.1509	<b>0.8736</b>	<b>1.0842</b>	<b>0.0655</b>	<b>0.0539</b>
TiRex	0.9682	<u>1.1934</u>	0.1518	0.1243	2.0462	2.4235	0.1346	0.1134	<b>1.8559</b>	2.2147	0.1894	0.1422	1.0314	1.3493	0.0820	0.0677
Toto-1.0	1.0364	1.2804	0.1784	0.1439	2.1277	2.5080	0.1511	0.1223	2.0094	2.2865	0.1978	0.1392	1.1139	1.4307	0.0947	0.0770
Ours	<u>0.9596</u>	1.2168	0.1550	0.1247	<u>1.9960</u>	<u>2.3642</u>	<b>0.1259</b>	<b>0.0982</b>	1.9776	2.1875	0.1571	<u>0.1215</u>	1.0562	1.2099	0.0801	0.0676

Table 15. Performance Comparison on solar\_with\_weather\_15T and solar\_with\_weather\_1H. The best results are highlighted in **bold**, and the second-best results are underlined.

Model	15T				1H			
	SQL	MASE	WAPE	WQL	SQL	MASE	WAPE	WQL
AutoARIMA	—	—	—	—	1.1314	1.1133	1.2902	1.2703
AutoETS	2.5289	2.4162	1.4215	1.9572	2.1818	2.2682	1.1465	1.3928
AutoTheta	3.5851	1.2729	1.5023	3.2873	3.3576	1.5354	1.5474	2.6715
Chronos-Bolt	0.8094	0.9765	1.2911	1.1301	0.8157	1.0720	1.3260	1.0190
Moirai-2.0	0.8387	1.0764	1.3761	1.1205	0.9071	1.1358	1.4828	1.2285
Naive	2.2780	1.9895	<b>1.0180</b>	1.6964	2.1807	2.2682	1.1464	1.3916
Seasonal Naive	1.1938	1.0501	1.3115	1.4074	1.2120	1.0619	1.2339	1.3171
Stat. Ensemble	—	—	—	—	1.4584	1.3148	1.2682	1.1488
Sundial-Base	0.9626	1.1182	1.5059	1.3508	1.1815	1.3032	1.4481	1.3598
TabPFN-TS	<u>0.7471</u>	0.9445	1.1662	<u>0.9712</u>	<u>0.7006</u>	<b>0.8629</b>	<b>0.9096</b>	<b>0.7960</b>
TimesFM-2.5	0.9063	1.1153	1.4700	1.2405	0.8154	1.0513	1.2011	0.9696
TiRex	0.8457	1.0487	1.4236	1.2068	0.9000	1.1583	1.5261	1.2499
Toto-1.0	0.7839	<u>0.9403</u>	1.1480	0.9998	0.8760	1.0585	1.4068	1.2191
Ours	<b>0.7402</b>	<b>0.8951</b>	<u>1.0609</u>	<b>0.8912</b>	<b>0.6751</b>	<u>0.8774</u>	<u>1.0128</u>	<u>0.8174</u>

Table 16. Performance Comparison on uci\_air\_quality\_1H and uci\_air\_quality\_1D. The best results are highlighted in **bold**, and the second-best results are underlined.

Model	1H				1D			
	SQL	MASE	WAPE	WQL	SQL	MASE	WAPE	WQL
AutoARIMA	1.1924	1.3698	0.4518	0.3924	1.2403	1.5585	0.3229	0.2530
AutoETS	$4.10 \times 10^5$	10.6979	4.0642	$2.05 \times 10^5$	1.1813	<b>1.3629</b>	<b>0.2791</b>	0.2425
AutoTheta	1.9560	1.3458	0.4168	0.6724	1.2334	1.4428	0.2964	0.2579
Chronos-Bolt	0.8990	1.1162	0.3758	0.3020	<b>1.0920</b>	1.3887	<u>0.2843</u>	<b>0.2229</b>
Moirai-2.0	0.9454	1.1965	0.3904	0.3063	1.1380	1.4417	0.2916	<u>0.2299</u>
Naive	2.4250	1.6816	0.5251	0.8361	1.8739	2.1091	0.4315	0.3990
Seasonal Naive	1.3840	1.4425	0.4563	0.4609	1.4013	1.7337	0.3624	0.2922
Stat. Ensemble	1.5607	1.2992	0.4116	0.5269	1.1225	1.3837	0.2860	0.2304
Sundial-Base	1.0009	1.1924	0.4007	0.3369	1.2145	1.3991	0.2893	0.2497
TabPFN-TS	0.9312	1.1751	0.3858	0.3067	1.1863	1.5308	0.3106	0.2398
TimesFM-2.5	0.8769	1.1226	0.3715	0.2904	1.2051	1.5147	0.3069	0.2425
TiRex	<b>0.8650</b>	<b>1.1062</b>	0.3698	0.2890	1.1280	1.4312	0.2942	0.2322
Toto-1.0	<u>0.8700</u>	<u>1.1112</u>	<b>0.3658</b>	<u>0.2863</u>	1.2602	1.5881	0.3233	0.2553
Ours	0.8732	1.1224	<u>0.3685</u>	<b>0.2794</b>	<u>1.1122</u>	<u>1.3667</u>	0.2881	0.2317

Table 17. Average results on load, photovoltaic, and all real application datasets. The best results are highlighted in **bold**, and the second-best results are underlined.

Model	Load datasets (18)				Photovoltaic datasets (9)				All real-world application datasets (27)			
	SQL	MASE	WAPE	WQL	SQL	MASE	WAPE	WQL	SQL	MASE	WAPE	WQL
AutoARIMA	2.5730	0.8526	0.0395	0.1289	3.5350	0.7858	0.2366	1.0570	2.8936	0.8303	0.1052	0.4383
AutoETS	7.4514	6.4652	0.2931	0.3218	22.4679	5.7401	1.7096	6.7013	12.4569	6.2235	0.7653	2.4483
AutoTheta	0.8977	1.2644	0.0632	0.0385	38.8877	6.6861	1.9921	11.5991	13.5611	3.0717	0.7062	3.8920
Chronos-Bolt	0.4415	<u>0.5491</u>	<u>0.0253</u>	<u>0.0203</u>	0.6471	0.8066	0.2424	0.1945	0.5101	0.6350	0.0976	0.0783
Moirai-2.0	0.7621	0.9701	0.0460	0.0360	0.6175	0.7222	0.2175	0.1859	0.7139	0.8875	0.1031	0.0860
Naive	2.4675	3.0599	0.1479	0.1182	4.9932	5.7400	1.7095	1.4883	3.3094	3.9533	0.6684	0.5749
Seasonal Naive	1.0799	1.2065	0.0596	0.0499	6.2536	0.7382	0.2221	1.8697	2.8045	1.0504	0.1138	0.6565
Stat. Ensemble	1.6205	2.2320	0.1051	0.0760	3.2080	3.2719	0.9756	0.9570	2.1497	2.5786	0.3952	0.3696
Sundial-Base	0.7536	0.9411	0.0450	0.0360	0.7387	0.8304	0.2500	0.2225	0.7486	0.9042	0.1133	0.0981
TabPFN-TS	<u>0.5120</u>	0.6817	0.0325	0.0242	<u>0.3750</u>	<u>0.4710</u>	<u>0.1415</u>	<u>0.1127</u>	<u>0.4663</u>	<u>0.6115</u>	<u>0.0688</u>	<u>0.0537</u>
TimesFM-2.0	0.9410	1.0132	0.0506	0.0469	0.6434	0.7572	0.2266	0.1925	0.8418	0.9278	0.1093	0.0954
TiRex	0.5544	0.6896	0.0336	0.0270	0.6042	0.7490	0.2253	0.1813	0.5710	0.7094	0.0975	0.0784
Toto-1.0	0.8888	1.1359	0.0557	0.0430	0.7465	0.8981	0.2694	0.2241	0.8414	1.0566	0.1269	0.1034
Ours	<b>0.4089</b>	<b>0.5182</b>	<b>0.0219</b>	<b>0.0174</b>	<b>0.3743</b>	<b>0.4504</b>	<b>0.1352</b>	<b>0.1121</b>	<b>0.3974</b>	<b>0.4956</b>	<b>0.0597</b>	<b>0.0490</b>

Table 18. Summary of the 10 representative univariate forecasting tasks selected from fev-bench-mini, collectively referred to as fev-bench-uni. Datasets with multiple targets (# targets > 1) are decomposed into independent univariate series for evaluation.

Task	Domain	Frequency	# items	median length	# obs	# known dynamic cols	H	W	# seasonality	# targets
ETT_15T	energy	15 Min	2	69,680	975,520	0	96	20	96	7
ETT_1H	energy	1 H	2	17,420	243,880	0	168	20	24	7
bizitobs_l2c_5T	cloud	5 Min	1	31,968	223,776	0	288	20	288	7
boomlet_619	cloud	1 Min	1	16,384	851,968	0	60	20	1440	52
boomlet_l282	cloud	1 Min	1	16,384	573,440	0	60	20	1440	35
boomlet_l676	cloud	30 Min	1	10,463	1,046,300	0	96	20	48	100
hospital_admissions_1D	healthcare	Daily	8	1,731	13,846	0	28	20	7	1
hospital_admissions_1W	healthcare	Weekly	8	246	1,968	0	13	16	1	1
jena_weather_1H	nature	1 H	1	8,784	184,464	0	24	20	24	21
M_DENSE_1D	mobility	Daily	30	730	21,900	0	28	10	7	1

to univariate time series forecasting, we formulate the input with a dummy covariate (e.g., a column of zeros) alongside intrinsic temporal features such as year, month, day, and hour to preserve compatibility with the model’s covariate-aware architecture. Despite the absence of meaningful external covariates, Baguan-TS exhibits highly competitive performance on univariate forecasting tasks. Notably, it achieves best results in both WAPE and WQL (see Table 19 and Fig. 21). This strong performance underscores the model’s robustness in capturing distributional characteristics and its reliability in high-stakes or extreme-value scenarios, where WAPE emphasizes large errors proportionally to actual magnitudes, and WQL explicitly optimizes quantile-based risk awareness. Detailed experimental results are presented in Tables 20–23.

Table 19. Average results on fev-bench-uni. The best results are highlighted in bold.

Model	SQL	MASE	WAPE	WQL
Chronos-Bolt	0.6083	0.7369	0.3974	0.3438
Moirai-2.0	<b>0.5405</b>	<b>0.6728</b>	0.3254	0.2735
Sundial-Base	0.5814	0.6833	0.3338	0.2902
TabPFN-TS	0.5920	0.7364	0.3384	0.2685
TimesFM-2.5	0.5428	0.6831	0.3341	0.2726
TiRex	0.5684	0.7104	0.3858	0.3215
Toto-1.0	0.5689	0.7147	0.3635	0.2992
AutoARIMA	0.6913	0.8301	0.5843	0.5548
Stat. Ensemble	0.7575	0.8371	0.5132	0.5844
AutoETS	0.9083	0.9519	0.4877	0.6018
AutoTheta	0.9409	0.8532	0.4972	0.6327
Seasonal Naive	1.0381	1.0373	0.6649	0.7433
Naive	1.3600	1.0902	0.5254	0.7872
Ours	0.5664	0.7126	<b>0.3105</b>	<b>0.2497</b>

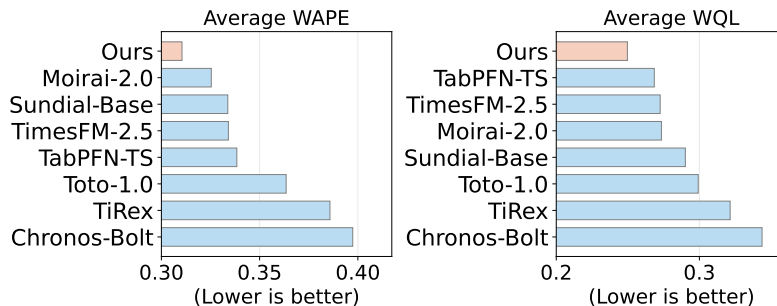


Figure 21. Probabilistic forecasting evaluation on fev-bench-uni using WAPE and WQL.

Table 20. Performance Comparison on ETT\_15T and ETT\_1H. The best results are highlighted in **bold**, and the second-best results are underlined.

Model	15T				1H			
	SQL	MASE	WAPE	WQL	SQL	MASE	WAPE	WQL
AutoARIMA	—	—	—	—	1.0524	1.2616	0.2730	0.2275
AutoETS	1.2626	1.4293	0.2090	0.1890	1.7645	1.6021	0.3240	0.3554
AutoTheta	1.0985	0.8022	0.1328	0.1702	2.0613	1.2847	0.2708	0.3879
Chronos-Bolt	0.5737	<b>0.7033</b>	<b>0.1146</b>	0.0933	0.9436	1.1267	0.2465	0.2059
Moirai-2.0	<b>0.5634</b>	<u>0.7119</u>	0.1160	<b>0.0915</b>	0.8993	1.1240	0.2470	0.1952
Naive	1.3269	1.3671	0.2028	0.2051	2.3137	1.7184	0.3389	0.4903
Seasonal Naive	0.7625	0.9169	0.1473	0.1224	1.2069	1.3227	0.2864	0.2597
Stat. Ensemble	—	—	—	—	1.2717	1.2519	0.2621	0.2620
Sundial-Base	0.5971	0.7139	<u>0.1157</u>	0.0970	0.9634	1.1439	0.2548	0.2147
TabPFN-TS	0.6024	0.7625	0.1222	0.0966	0.9332	1.1774	0.2553	0.2034
TimesFM-2.5	0.5772	0.7295	0.1167	<u>0.0925</u>	0.8823	1.1239	<u>0.2452</u>	<u>0.1916</u>
TiRex	<u>0.5683</u>	0.7188	0.1158	<b>0.0915</b>	<u>0.8736</u>	<u>1.1178</u>	0.2477	0.1924
Toto-1.0	0.5930	0.7578	0.1216	0.0952	<b>0.8727</b>	<b>1.1129</b>	<b>0.2432</b>	<b>0.1900</b>
Ours	0.6121	0.7810	0.1253	0.0980	0.9036	1.1549	0.2566	0.2022

 Table 21. Performance Comparison on hospital\_admissions\_1D and hospital\_admissions\_1W. The best results are highlighted in **bold**, and the second-best results are underlined.

Model	1D				1W			
	SQL	MASE	WAPE	WQL	SQL	MASE	WAPE	WQL
AutoARIMA	0.5556	0.7209	0.5348	0.4122	0.5793	<u>0.7541</u>	<b>0.2123</b>	0.1631
AutoETS	0.5558	0.7211	0.5350	0.4123	<b>0.5783</b>	<u>0.7541</u>	<b>0.2123</b>	<b>0.1628</b>
AutoTheta	0.5748	0.7429	0.5510	0.4264	0.5977	0.7779	0.2191	0.1683
Chronos-Bolt	0.5562	0.7195	0.5337	0.4125	0.5868	0.7623	0.2146	0.1653
Moirai-2.0	0.5556	0.7188	0.5332	0.4121	0.5862	0.7643	0.2153	0.1652
Naive	1.3251	0.9747	0.7243	0.9837	1.0492	1.0436	0.2934	0.2969
Seasonal Naive	0.8572	1.0268	0.7622	0.6361	1.0492	1.0436	0.2934	0.2969
Stat. Ensemble	0.5570	0.7214	0.5352	0.4131	<u>0.5789</u>	0.7552	0.2126	<u>0.1630</u>
Sundial-Base	0.6103	0.7225	0.5359	0.4526	0.6411	0.7599	0.2139	0.1802
TabPFN-TS	0.5623	0.7245	0.5375	0.4171	0.5814	<b>0.7534</b>	<b>0.2123</b>	0.1638
TimesFM-2.5	0.5561	0.7193	0.5336	0.4125	0.5795	0.7545	<u>0.2124</u>	0.1632
TiRex	<u>0.5551</u>	0.7180	0.5326	<u>0.4118</u>	0.5851	0.7610	0.2142	0.1648
Toto-1.0	0.5555	<u>0.7173</u>	<u>0.5321</u>	0.4120	0.5976	0.7781	0.2188	0.1681
Ours	<b>0.5546</b>	<b>0.7167</b>	<b>0.5317</b>	<b>0.4114</b>	0.6488	0.8405	0.2368	0.1827

 Table 22. Performance Comparison on boomlet\_619, boomlet\_1676, and boomlet\_1282. The best results are highlighted in **bold**, and the second-best results are underlined.

Model	619				1676				1282			
	SQL	MASE	WAPE	WQL	SQL	MASE	WAPE	WQL	SQL	MASE	WAPE	WQL
AutoARIMA	0.5545	0.7170	0.5880	0.4527	—	—	—	—	0.5565	0.5925	0.4050	0.3750
AutoETS	0.8944	1.0938	0.9529	0.7636	0.7564	0.7610	0.3540	0.3561	0.9136	0.6890	0.4705	0.6261
AutoTheta	0.8352	1.0200	0.8821	0.6993	0.7835	0.7772	0.3606	0.3690	0.9717	0.6910	0.4718	0.6673
Chronos-Bolt	0.4709	0.5941	0.4683	0.3764	0.6077	0.7192	0.3289	0.2758	0.4618	0.5647	0.3918	0.3174
Moirai-2.0	<u>0.3294</u>	0.4306	0.3062	0.2356	0.5727	0.7128	0.3274	0.2580	0.4269	0.5230	0.3639	0.2944
Naive	1.2752	1.1236	0.9459	0.9679	1.3196	0.8199	0.3738	0.5376	1.5394	0.8299	0.5674	1.0473
Seasonal Naive	1.2752	1.1236	0.9459	0.9679	0.8504	0.9529	0.4490	0.3899	1.5394	0.8299	0.5674	1.0473
Stat. Ensemble	0.7772	1.0047	0.8714	0.6586	—	—	—	—	0.7391	0.6398	0.4330	0.4977
Sundial-Base	0.3705	0.4356	0.3110	0.2649	0.6146	0.7138	0.3250	0.2744	0.4522	0.5169	0.3604	0.3126
TabPFN-TS	0.3305	<u>0.4305</u>	<u>0.3036</u>	<u>0.2349</u>	0.8311	0.9587	0.3439	0.2853	0.4253	0.5067	0.3518	0.2921
TimesFM-2.5	0.3398	0.4364	0.3117	0.2458	<u>0.5626</u>	<u>0.6982</u>	<u>0.3195</u>	<u>0.2520</u>	<b>0.4034</b>	<b>0.4938</b>	<b>0.3418</b>	<b>0.2770</b>
TiRex	0.3411	0.4418	0.3174	0.2471	0.5712	0.7093	0.3220	0.2548	0.4089	<u>0.4966</u>	0.3447	0.2814
Toto-1.0	<b>0.3099</b>	<b>0.4032</b>	<b>0.2789</b>	<b>0.2163</b>	<b>0.5544</b>	<b>0.6907</b>	<b>0.3174</b>	<b>0.2495</b>	<u>0.4069</u>	0.4983	<u>0.3444</u>	<u>0.2786</u>
Ours	0.3399	0.4391	0.3128	0.2445	0.6195	0.7691	0.3482	0.2760	0.4169	0.5077	0.3529	0.2877

Table 23. Performance Comparison on bizitobs\_12c\_5T, jena\_weather\_1H, and M\_DENSE\_1D. The best results are highlighted in **bold**, and the second-best results are underlined.

Model	bizitobs_12c_5T				jena_weather_1H				M_DENSE_1D			
	SQL	MASE	WAPE	WQL	SQL	MASE	WAPE	WQL	SQL	MASE	WAPE	WQL
AutoARIMA	0.8247	0.9163	1.5980	1.8772	0.4370	0.5092	0.9375	0.8257	0.9702	1.1690	0.1261	0.1051
AutoETS	0.7311	0.8137	1.3367	1.6114	0.5529	0.5678	0.3522	1.4085	1.0735	1.0869	0.1301	0.1324
AutoTheta	0.7496	0.8740	1.6561	1.6069	0.5933	0.4846	0.2955	1.6859	1.1435	1.0772	0.1322	0.1459
Chronos-Bolt	0.7570	0.8002	1.3254	1.2750	0.3668	0.4543	0.2519	0.2341	0.7590	0.9249	0.0985	0.0817
Moirai-2.0	<b>0.3675</b>	<b>0.4035</b>	0.7997	0.7682	0.3652	0.4505	<u>0.2487</u>	0.2342	0.7390	<u>0.8884</u>	0.0962	0.0807
Naive	0.6779	0.7578	1.2819	1.4508	0.5789	0.5375	0.3286	1.6602	2.1937	1.7292	0.1970	0.2323
Seasonal Naive	0.9226	1.0667	2.2838	2.2878	0.6550	0.7399	0.7712	1.2878	1.2627	1.3500	0.1420	0.1368
Stat. Ensemble	0.7197	0.8069	1.3437	1.5129	0.4516	0.4664	0.3279	1.0549	0.9648	1.0509	0.1193	0.1131
Sundial-Base	<u>0.4004</u>	<u>0.4808</u>	<u>0.6893</u>	<u>0.5858</u>	0.3803	0.4459	0.4352	0.4351	0.7845	0.9000	0.0968	0.0844
TabPFN-TS	0.4855	0.6193	0.8823	0.6797	0.4128	0.5111	0.2825	0.2343	0.7560	0.9195	<b>0.0927</b>	<u>0.0776</u>
TimesFM-2.5	0.4611	0.5787	0.9057	0.7905	<u>0.3589</u>	<u>0.4392</u>	0.2604	0.2233	<b>0.7075</b>	<b>0.8576</b>	<u>0.0935</u>	<b>0.0774</b>
TiRex	0.6789	0.7959	1.4136	1.2725	<b>0.3557</b>	<b>0.4379</b>	0.2507	<u>0.2168</u>	0.7460	0.9066	0.0993	0.0822
Toto-1.0	0.5954	0.7136	1.2221	1.0847	0.3616	0.4476	<b>0.2468</b>	<b>0.2069</b>	0.8418	1.0279	0.1093	0.0907
Ours	0.4360	0.5379	<b>0.5545</b>	<b>0.4372</b>	0.3949	0.4827	0.2883	0.2758	<u>0.7374</u>	0.8962	0.0976	0.0812